Kroll, E., Bayon, C., Rudd, J. J., Armer, V., Magaji-Umashankar, A., Ames, R., Urban, M., Brown, N. A. and Hammond-Kosack, K. E. 2025. A conserved fungal Knr4/Smi1 protein is vital for maintaining cell wall integrity and host plant pathogenesis . *PLOS Pathogens.* 21 (1), p. e1012769. https://doi.org/10.1371/journal.ppat.1012769

PLOS PATHOGENS

RESEARCH ARTICLE

A conserved fungal Knr4/Smi1 protein is crucial for maintaining cell wall stress tolerance and host plant pathogenesis

Erika Kroll[1,2], **Carlos Bayon**[1], **Jason Rudd**[1], **Victoria J. Armer**[1], **Anjana Magaji-Umashankar**[1], **Ryan Ames**[3], **Martin Urban**[1], **Neil A. Brown**[2], **Kim Hammond-Kosack**[1]*

1 Strategic Area: Protecting Crops and the Environment, Rothamsted Research, Harpenden, Hertfordshire, United Kingdom, **2** Department of Life Sciences, University of Bath, Bath, Somerset, United Kingdom, **3** Biosciences and Living Systems Institute, University of Exeter, Devon, Exeter, United Kingdom

* kim.hammond-kosack@rothamsted.ac.uk

Citation: Kroll E, Bayon C, Rudd J, Armer VJ, Magaji-Umashankar A, Ames R, et al. (2025) A conserved fungal Knr4/Smi1 protein is crucial for maintaining cell wall stress tolerance and host plant pathogenesis. PLoS Pathog 21(1): e1012769. https://doi.org/10.1371/journal.ppat.1012769

Editor: Jin-Rong Xu, Purdue University, UNITED STATES OF AMERICA

Received: September 13, 2024

Accepted: November 22, 2024

Published: January 9, 2025

Data Availability Statement: All input raw RNA-seq count files, code used for the network analysis, and full lists of all genes clustered into modules is available on https://github.com/erikakroll/Fusarium-wheat_WGCNA and have been deposited on the repository HARVESTIRR (https://doi.org/10.23637/rothamsted.99163). The full gene lists includes comma separated value (CSV) files for all genes in each module for both fungal and wheat modules, which are annotated with Module Membership (MM) values, mean FPKM values, InterPro annotation, Gene Ontology annotation,

Abstract

Filamentous plant pathogenic fungi pose significant threats to global food security, particularly through diseases like Fusarium Head Blight (FHB) and Septoria Tritici Blotch (STB) which affects cereals. With mounting challenges in fungal control and increasing restrictions on fungicide use due to environmental concerns, there is an urgent need for innovative control strategies. Here, we present a comprehensive analysis of the stage-specific infection process of *Fusarium graminearum* in wheat spikes by generating a dual weighted gene co-expression network (WGCN). Notably, the network contained a mycotoxin-enriched fungal module (F12) that exhibited a significant correlation with a detoxification gene-enriched wheat module (W12). This correlation in gene expression was validated through quantitative PCR. By examining a fungal module with genes highly expressed during early symptomless infection that was correlated to a wheat module enriched in oxidative stress genes, we identified a gene encoding FgKnr4, a protein containing a Knr4/Smi1 disordered domain. Through comprehensive analysis, we confirmed the pivotal role of FgKnr4 in various biological processes, including oxidative stress tolerance, cell cycle stress tolerance, morphogenesis, growth, and pathogenicity. Further studies confirmed the observed phenotypes are partially due to the involvement of FgKnr4 in regulating the fungal cell wall integrity pathway by modulating the phosphorylation of the MAP-kinase MGV1. Orthologues of the *FgKnr4* gene are widespread across the fungal kingdom but are absent in other Eukaryotes, suggesting the protein has potential as a promising intervention target. Encouragingly, the restricted growth and highly reduced virulence phenotypes observed for *ΔFgknr4* were replicated upon deletion of the orthologous gene in the wheat fungal pathogen *Zymoseptoria tritici*. Overall, this study demonstrates the utility of an integrated network-level analytical approach to pinpoint genes of high interest to pathogenesis and disease control.

and Trait Ontology annotation. Text documents containing module eigengene values and gene module assignments are also available on the repository.

Funding: This study was supported by funding from the Biotechnology and Biological Sciences Research Council (BBSRC, https://www.ukri.org/councils/bbsrc/), including the South West Biosciences Doctoral Training Partnership grant BB/T008741/1 (E.K. and V.J.A.); the Designing Future Wheat programme, grants BBS/E/C/000I0250 (K.H.K., M.U., J.R., and C.B.) and Delivering Sustainable Wheat, grants BB/X011003/1 and BBS/E/RH/230001B (K.H.K., M.U., J.R., and C.B.); the Growing Health grant BB/X010953/1 (J. R. and C.B.); and additional BBSRC grants BB/X012131/1 and BB/W007134/1 (K.H.K. and M.U.). N.A.B was supported by the BBSRC Future Leader Fellowship BB/N011686/1. R.A was supported by a BBSRC/EPSRC (Biotechnology and Biological Sciences Research Council/ Engineering and Physical Sciences Research Council) Interface Innovation Fellowship (EP/S001352/1) (https://www.ukri.org/councils/bbsrc/; https://www.ukri.org/councils/epsrc/).The funders did not play a role in the study design, data collection and analysis, decision to publish, or preparation of the manuscript.

Competing interests: The authors have declared that no competing interests exists.

Author summary

Filamentous fungi, including *Fusarium graminearum* and *Zymoseptoria tritici*, pose serious threats to global food security by causing devastating diseases in cereal crops, including wheat, a key staple food. With growing challenges in control due to increased fungicide resistance and heightened restrictions on fungicide use due to environmental concerns, the need for innovative control strategies has become urgent. This study presents a dual weighted gene co-expression network (WGCN) analysis of the infection process of *F. graminearum* in wheat. The analysis found a fungal module (F16) which was uniquely highly expressed during the earliest stages of fungal colonisation and was correlated with a wheat module enriched in oxidative stress defence related genes. A key fungal gene of module F16, *FgKnr4*, was identified as crucial for oxidative stress tolerance, cell cycle stress tolerance, morphogenesis, and full virulence. Promisingly, the *Knr4* gene is highly conserved and specific to the fungal kingdom. Disruption of the *Knr4* orthologue in *Zymoseptoria tritici* led to parallel phenotypes of reduced fungal growth, cell wall stress tolerance, and virulence. These findings suggest that *FgKnr4* could serve as a potential target for controlling fungal diseases in crops, highlighting the power of network-based approaches in identifying genes essential to fungal pathogenesis.

Introduction

The wheat crop (*Triticum* species) plays a crucial role in global food security, contributing about 20% of dietary calories and protein worldwide [1], while also supplying essential nutrients and bioactive food components [2]. Pathogen and pest burden substantially contribute to wheat losses globally, accounting for ~21.5% of wheat losses annually [3]. Of these, the five highest global contributors to wheat yield and quality losses are all fungal diseases and include Fusarium Head Blight disease (FHB) and Septoria tritici blotch disease (STB), which account for 2.85% and 2.44% of wheat losses, respectively [3].

FHB is a mycotoxigenic pre-harvest fungal disease of most cereals, caused by different *Fusaria* within the *Fusarium sambucinum* species complex that is increasingly prevalent in most cereal growing regions globally [4–7]. Floral infections lead to contamination of grain with mycotoxins that are subject to strict legal limits in different global regions [8–10]. Despite ongoing endeavours to manage FHB, mycotoxin contamination continues to significantly impact the economies of cereal and livestock producers, as well as the food, drink, and feed industries [11]. The B-type sesquiterpenoid deoxynivalenol (DON) is the most common FHB mycotoxin in European food and feed wheat [6]. The globally predominant DON producing species is *Fusarium graminearum* [4]. During wheat spike colonisation, *F. graminearum* undergoes a biphasic mode of infection. Initially, the fungus evades the host immune response by growing between cells, causing no visible symptoms for ~3 days. This is followed by an extended symptomatic stage marked by wheat tissue bleaching and reduced grain development behind the advancing hyphal front [12,13]. STB disease on wheat leaves is caused by the fungus *Zymoseptoria tritici*. This fungus has an extended symptomless stage of infection ~9 days, followed by a switch to symptomatic disease [14,15]. However, unlike *F. graminearum*, *Z. tritici* colonisation is strictly confined to the sub-stomatal cavities and apoplastic spaces, without ever invading host cells [16]. Both pathogens are currently managed using semi effective sources of host resistance mediated by major genes or QTLs [17–19] as well as fungicide applications [5,19,20,21]. But effective control faces escalating issues caused by fungicide

resistance [22–25]. There is a critical need to develop new methods to combat these and other wheat fungal pathogens.

Understanding the genetic and molecular mechanisms driving host infection in numerous interaction types continues to be a major goal of the international molecular plant pathology community [26,27]. Gene expression data can be organised into co-expression networks, which group genes based on shared co-expression patterns. Network representations are advantageous because these present biological data on a systems-wide level, clustering genes in modules representative of specific stages or functions. Previous network analyses in *F. graminearum* have included two comprehensive gene regulatory networks (GRNs) based on Affymetrix gene expression datasets, which combined both *in vitro* and *in planta* datasets [28,29]. However, out of the >12 datasets used in these studies, only one examined the infection of wheat spikes. As a consequence of this and the scale of the study, this analysis lacks the resolution needed to map genes to specific stages of *F. graminearum* infection. This high-resolution modelling can be achieved using the weighted gene co-expression network analysis (WGCNA) framework [30] to analyse a meticulously sampled, stage- and tissue-specific *in planta* RNA-seq dataset [31]. WGCNA has been repeatedly applied to analyse fungal gene expression data. For instance, this approach has been employed to identify effectors in *Magnaporthe oryzae* [32], shared genes during *Fusarium oxysporum* infection across multiple hosts [33], and virulence genes of *Colletotrichum siamense* [34]. Although WGCNA has been used to study wheat host responses to *F. graminearum* infection [35,36] and responses of *F. graminearum* under *in vitro* stress [37,38], there has been no study of wheat-*F. graminearum* co-expression profiles during infection.

To gain deeper insight on the expression patterns of genes during the different stages of the *F. graminearum* infection, the WGCNA framework was used to generate a fungal pathogen/wheat dual co-expression network. Significantly, this framework can facilitate the correlation of both fungal and host plant expression [39]. Within this approach, genes are grouped into modules based on shared co-expression patterns separately for the pathogen and the host. Modules are then correlated between the pathogen and host networks to predict shared expression dynamics. In this study, correlated expression between a mycotoxin gene-enriched fungal module and a detoxification gene-enriched wheat module, validated the host-pathogen network. The study then focused on the unique fungal module F16, characterised by high expression levels during the earliest symptomless infection stage and a correlation to a wheat module enriched in oxidative stress genes, which led to the discovery of *FgKnr4*. A subsequent comprehensive experimental analysis revealed the pivotal role of *FgKnr4* in various biological processes, including cell wall stress tolerance, cell cycle stress tolerance, morphogenesis, growth, and virulence in *F. graminearum*. The *Knr4* gene is not restricted to *F. graminearum* but is distributed widely across the fungal kingdom, but is absent in other Eukaryotes. The various mutant phenotypes observed in the *F. graminearum ΔFgknr4* strain were replicated upon deletion of the orthologous gene in the wheat pathogen *Z. tritici*. Overall, this study highlights the value of using network analyses to model spatio-temporal pathogen-host interactions and to identify novel conserved genes associated with virulence.

Results

Generation of a dual *F. graminearum*-wheat co-expression network

F. graminearum floral infections can be divided into symptomatic or symptomless stages of infection. Disease spread through the rachis internodes (RI) can be further broken down to four different key stages of infection. Namely early symptomless (RI7-8), late symptomless (RI5-6), early symptomatic (RI3-4), and late symptomatic (RI1-2) infection (**Fig 1A**). A

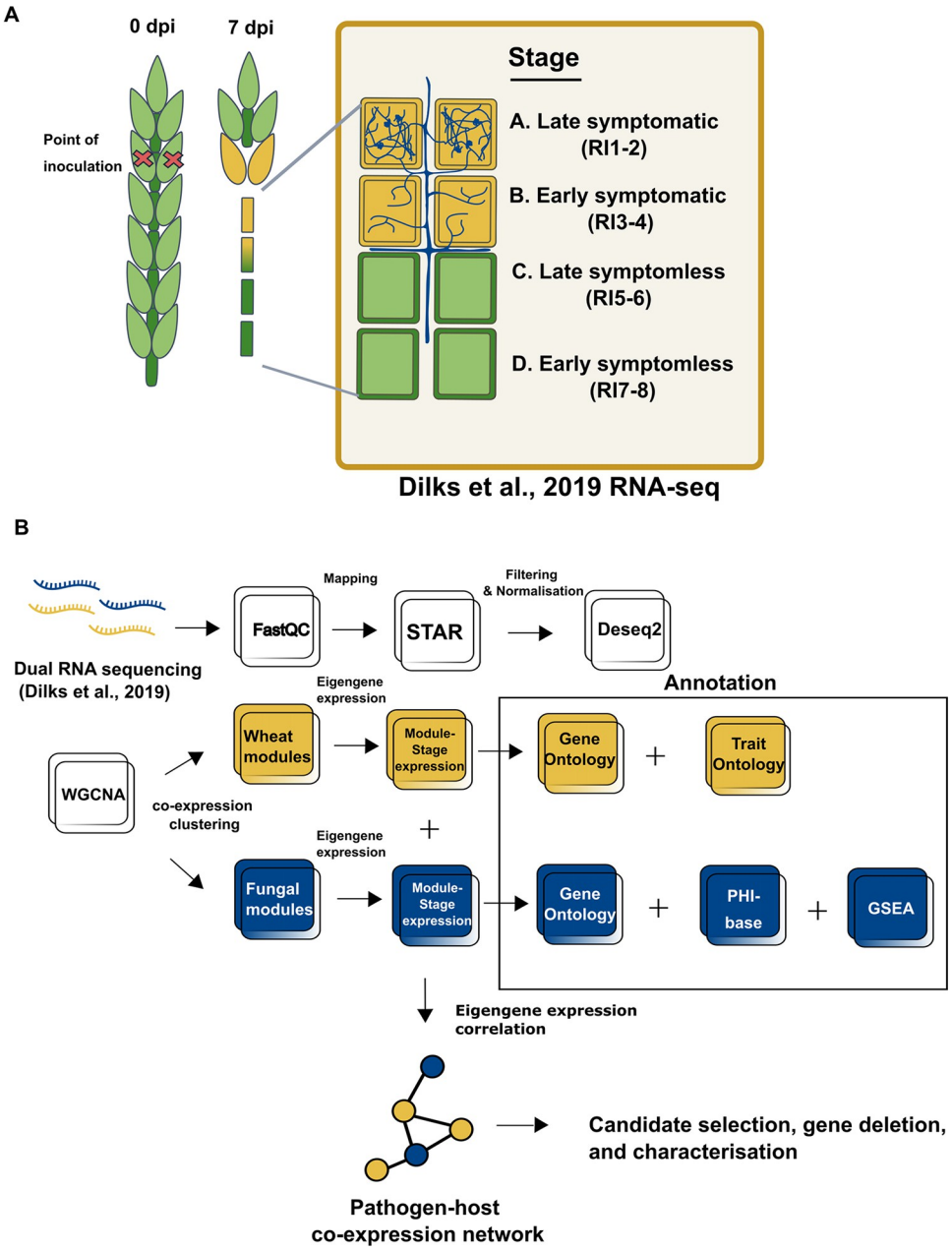

Fig 1. Dual RNA-seq dataset and bioinformatics pipeline used for constructing the dual co-expression network. **A.** Schematic illustration depicting the symptomatic (yellow) and symptomless (green) stages of *Fusarium graminearum* infection of wheat spikes denoted as stages A through D, corresponding to tissue samples collected for generating the RNA-seq data published in Dilks et al. 2019 [31]. *F. graminearum* hyphae growing in either the apoplast or inside the wheat cells are depicted in blue. **B.** Summary outlining the bioinformatics pipeline used for processing raw reads and constructing the dual RNA-seq network. The dual RNA-seq reads were initially processed together (processes depicted as white squares) before being separated to generate two distinct weighted gene co-expression networks. The bioinformatic pipelines are annotated accordingly, with yellow indicating the wheat reads-only pipeline and blue indicating the fungal reads-only pipeline. Annotation includes Gene Ontology terms (GO), Trait Ontology terms (TO), unique Gene Set Enrichment Analysis (GSEA), and PHI-base phenotypes. The modules from the two separate networks are then correlated to each other by their eigengene values to form the dual co-expression network.

https://doi.org/10.1371/journal.ppat.1012769.g001

spatio-temporal transcriptomics dataset of *F. graminearum* floral infection of the susceptible wheat cultivar Bobwhite, which distinguishes between these key distinct stages, was previously generated [31]. This dataset also included spikelet tissue (SP) sampled at 3 (early symptomatic) and 7 days post-infection (dpi) (late symptomatic). The WGCNA framework [40,30] was used to construct a dual co-expression network to model fungal pathogen/crop interaction in wheat using this dataset **(Fig 1B)**.

Normalised counts were used to generate two distinct networks: one for *F. graminearum* and another for *T. aestivum*. The *F. graminearum* network consisted of 10,189 genes organised into 18 modules (with 2629–60 genes per module), while the *T. aestivum* network consisted of 47,458 genes distributed among 25 modules (with 23063–83 genes per module) **(Figs 2A, S1 and S1 File)**. Both networks met scale free model criteria at their selected soft thresholding power **(S2A and S2B Fig)**. The examination of module quality statistics found that each module within both networks were of a high quality (Z-Summary > 10), with the exception of F16 (Z-Summary = 9.67), which still markedly surpasses the minimum Z-Summary score of > 2 [41] **(S2C Fig)**. This indicates a substantial preservation of modules compared to a random selection of all network genes. Additionally, preservation statistic calculations confirmed that all modules maintain preservation (Z-summary > 2) across both networks with all modules of the wheat network and the majority of the fungal modules (11/18) having strong preservation (Z-summary > 10) **(S2D Fig)**. These findings suggest a consistent preservation of within-network topology across modules [41]. For each module, a single summarised expression pattern, the eigengene value, was calculated. The fungal and wheat modules were correlated by their eigengene expression values, and modules displaying significant correlation ($p \leq 0.001$) formed the dual co-expression network **(Fig 2A and 2B)**.

To gain insight into the function of individual modules, a Gene Ontology (GO) enrichment analysis was performed for both network sets **(Figs 2D, 2E and S1)**. To confirm these enrichment patterns were not due to chance, a random network was generated for both the fungal and wheat datasets. No significant enrichment was found for the random wheat network and fungal network.

Among the eight wheat modules within the dual co-expression network, five of them were significantly enriched for disease resistance genes (TO:0000112, $p \leq 0.05$) and one was specifically enriched for wheat stripe rust resistance genes (TO:0020055) **(Fig 2D)**, suggesting the wheat modules in the network are needed for plant defence. One of these wheat modules, W12, was significantly enriched in the GO terms detoxification (GO:0098754; $p = 7.13 \times 10^{-7}$) and response to toxic substances (GO:0009636; $p = 2.11 \times 10^{-6}$). This module was correlated to the fungal module F12, which was enriched in genes belonging to the trichothecene biosynthesis (*TRI)* gene cluster (*TRI3*, *TRI4*, *TRI11*, *TRI12*, and *TRI14)* ($p = 1.92 \times 10^{-4}$) and for the GO term terpenoid biosynthesis (GO:0016114; $p = 0.00085$) **(Fig 2E and Table 1)**.

The stage specific expression patterns of each module was examined **(Figs 3, S3 and S4)**. Notably, the expression patterns of the *TRI* gene enriched module F12 aligned with its predicted function in DON biosynthesis. The module was most highly expressed in the late symptomless stage of infection. Expression of this module then rapidly decreased during the symptomatic stages of infection. Module F12 therefore appears to be positioned specifically at the transition between the late symptomless stage and the early symptomatic stage. The production of the DON mycotoxin is essential for the transition to the extensive symptomatic stage [52,53]. DON inhibits protein translation, which then eventually leads to cell death and the bleached phenotype distinctive of symptomatic *F. graminearum* infection [54,55]. High expression of module F12 in the symptomless stage is also supported by previous data which found that genes involved in mycotoxin biosynthesis are highly expressed in symptomless wheat tissue [56]. The correlation with the wheat module W12 therefore implies that

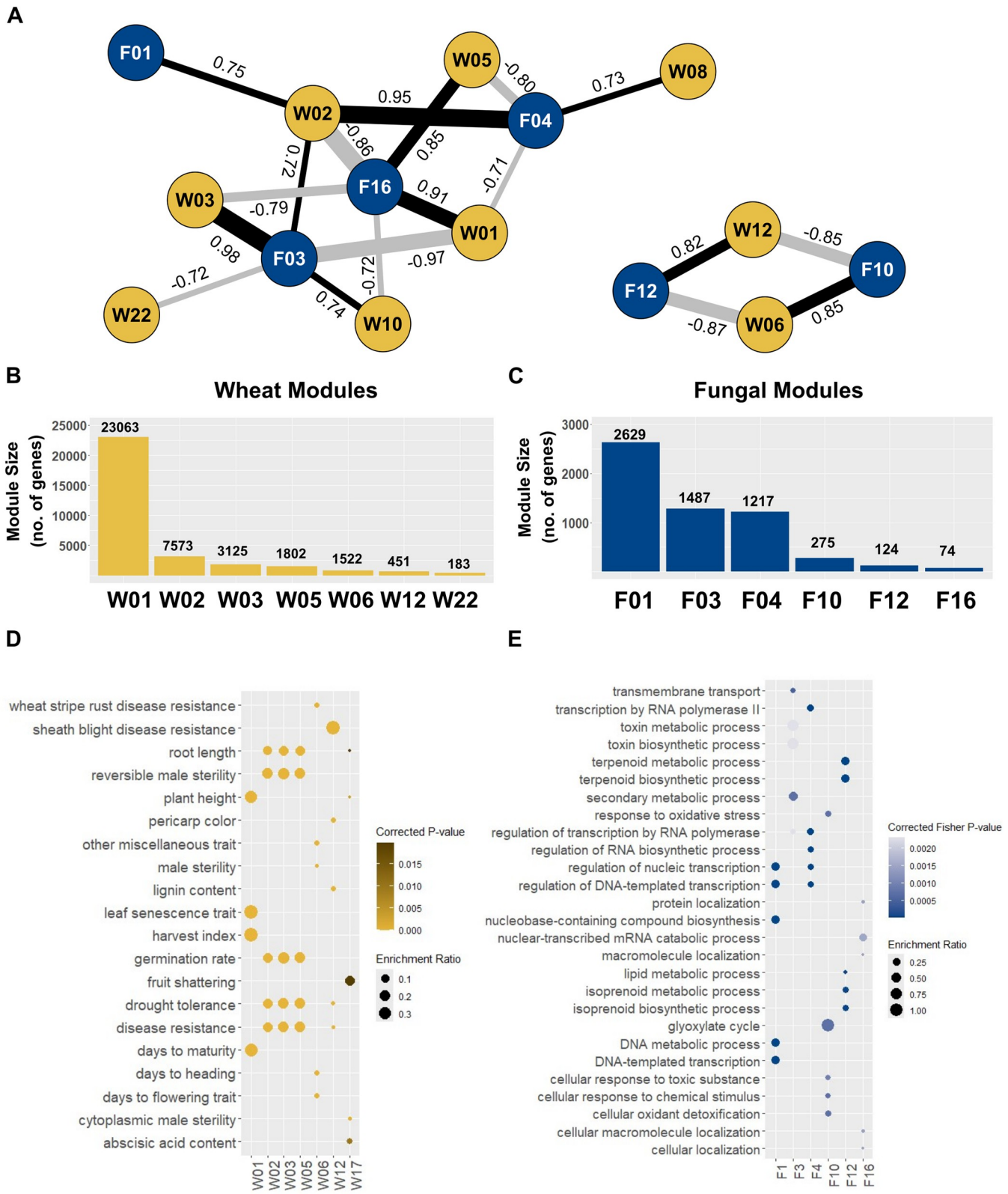

Fig 2. Dual Fungal-Wheat co-expression network. A. Network summarising significant co-expression patterns ($p \leq 0.001$) between fungal modules (blue nodes) and wheat modules (yellow nodes). Positive correlations are depicted as black edges, while negative correlations are shown as grey edges. R-squared values are indicated next to edges, with edge width corresponding to the value. **B.** Wheat modules sizes. **C.** Fungal module sizes (S1 File). **D. Wheat module**

enrichment. Significant Plant Trait Ontology (TO) enrichment results ($p \leq 0.05$) for the five most significant enrichment terms for all wheat modules in the network. Higher significance is indicated by brighter yellows. Sizes of the circles correspond to the enrichment ratio. **E. Fungal module enrichment.** Significant ($p \leq 0.05$) Biological Processes (BP) and Gene Ontology (GO) enrichment results for the five most significant terms of all fungal modules in the network. Higher significance is indicated by darker blues. Size of the circles correspond to the enrichment ratio.

https://doi.org/10.1371/journal.ppat.1012769.g002

detoxification genes in the module are being expressed in response to production of fungal mycotoxins.

Interestingly, the fungal module F10 contains genes that are highly expressed in the earliest and latest stages of *F. graminearum* infection, but not intermediate stages (**Fig 3**). The fungal module F10 includes the Killer toxin 4 genes (*KP4L*-1, KP4L-2, and KP4L-3). The *KP4L* genes are necessary for virulence and expressed during both self and non-self interactions (**Table 1**). It is suggested that KP4L proteins provide *F. graminearum* with a competitive advantage when occupying new niches [47], which would explain their expression during the earliest stage of infection. High expression during late infection may be necessary for intraspecific interactions, when the fungus is coordinating growth at a high fungal density.

The stress-responsive mitogen-activated protein kinase *FgOS-2* is a key regulator in *F. graminearum* and acts upstream of the ATF/CREB-activating transcription factor *FgAtf-1* (**Table 1**). Both *FgOS-2* and *FgAtf-1* cluster in module F10. These proteins are involved in broad functions, including secondary metabolite production, sexual reproduction, and stress

Table 1. Function of correlated expression between wheat and fungal modules. This table illustrates the relationship between wheat and fungal gene expression at different stages of infection, detailing the associated functions and key fungal genes involved.

Expression Stages	Wheat Module	Predicted function	Correlated Fungal Module	Fungal Genes	Fungal Gene Functions	References
Early symptomless stage of infection	W01	Maintenance genes (photosynthesis, RNA modification) and early defence response.	F16	*FgNPC1*	Regulation of membrane trafficking and sterol metabolism, which are essential for maintaining cellular integrity and function during the infection stages.	Breakspear et al. 2011 [42]
				Gzc2h045	Msn2 C2H2 transcription factor, associated with virulence and coordination of adaptation to environmental stressors including heat, osmotic, and oxidative stress.	Son et al., 2011 [43]; John et al., 2021 [44]
	W05	Disease resistance genes, including reactive oxygen species genes associated with programmed cell death response to restrict pathogen spread.		*GzCon7*	Msn2 C2H2 transcription factor, associated with virulence and regulation of cell wall biosynthesis.	Son et al., 2011 [43]; John et al., 2021 [44]
				FgSrp2	Pre-mRNA processing, alternative splicing, and virulence	Zhang et al., 2020 [45]
Early symptomless and late symptomatic stages of infection	W06	Enriched in protein catabolism and autophagy, involved in immune signalling, programmed cell death, and necrotrophic damage control.	F10	*KP4L-1*, *KP4L-2*, *KP4L-3*	Necessary for virulence, provide competitive advantage during new niche occupation, essential for intraspecific interactions at high fungal density	Lu and Faris, 2019 [46]; Vicente et al., 2022 [47]
				FgOS-2, *FgAtf-1*	Regulation of secondary metabolite production, sexual reproduction, and stress tolerance	Nguyen et al., 2013 [48]
				FgHyd3, *FgHyd5*	Attachment to hydrophobic surfaces, production of aerial mycelia	Shin et al., 2022 [49]
Late symptomless to early symptomatic	W12	Detoxification, response to toxic substances, and defence response.	F12	*TRI* genes (*TRI3*, *TRI4*, *TRI11*, *TRI12*, *TRI14*)	Production of DON mycotoxin needed for virulence.	Dyer et al., 2005 [50]; Kimura et al., 2007 [51]

https://doi.org/10.1371/journal.ppat.1012769.t001

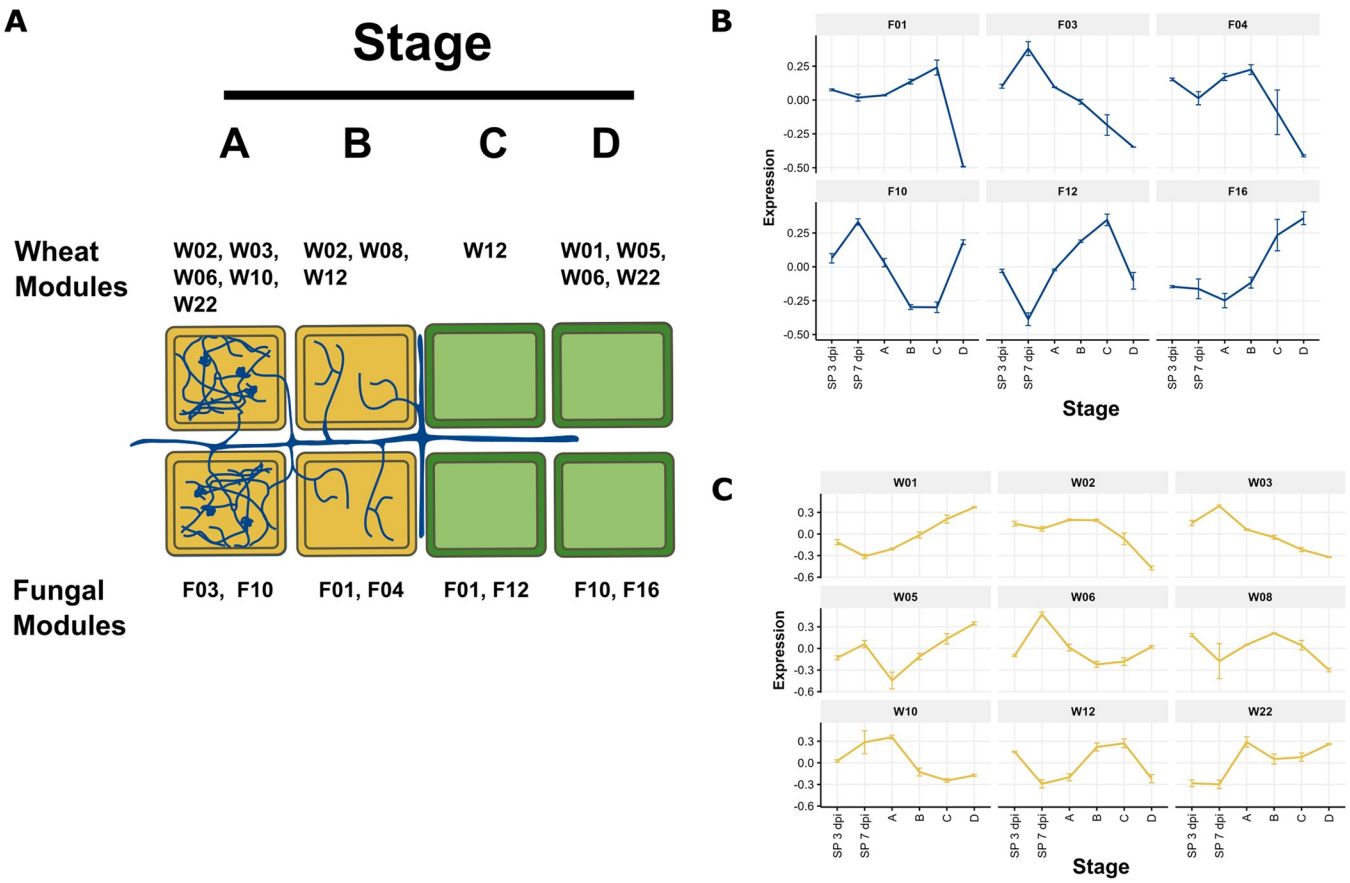

Fig 3. Stage-specific expression of modules in the dual co-expression network. A. Expression of modules across stages of *F. graminearum* infection. Illustration depicting symptomatic (yellow) and symptomless (green) stages of infection (A through D) annotated with specific modules (W or F) from the dual co-expression network that were highly expressed at specific stages. **B. Eigengene summarised expression of fungal modules** and **C. wheat modules**. Eigengene summarised expression plots illustrating the expression patterns of genes in wheat modules across different stages of infection as illustrated in panel A, along with spikelet tissue (SP) at 3 and 7 dpi.

https://doi.org/10.1371/journal.ppat.1012769.g003

tolerance [48]. Module F10 also contains two hydrophobin genes, *FgHyd3* and *FgHyd5*. *FgHyd3* is necessary for attachment to hydrophobic surfaces, while both genes are necessary for the production of aerial mycelia (**Table 1**). These genes are likely to play a crucial role during early infection for surface attachment and are possibly expressed again during the late stage of infection to facilitate the production of aerial mycelia.

The fungal module F10 is correlated with the wheat module W06 (R = 0.85, $p = 6 \times 10^{-6}$), which is enriched in protein catabolism (GO:0010498; $p = 1.60 \times 10^{-19}$) and autophagy (GO:0006914; $p = 2.31 \times 10^{-4}$) genes (**Table 1**). Autophagy plays a dual role in plant immunity where it is involved in immune signalling and programmed cell death to restrict pathogen spread, but also in response to pathogen induced necrotic cell death [57]. Therefore, it is likely these genes are expressed during early infection as an immediate immune response and then expressed again in highly colonised tissue for late-stage necrotrophic damage control.

Wheat genes in module W12 are expressed in response to DON production

To validate the correlation between modules F12 and W12, expression of wheat genes in the detoxification module W12 in response to *F. graminearum* infection with and without DON

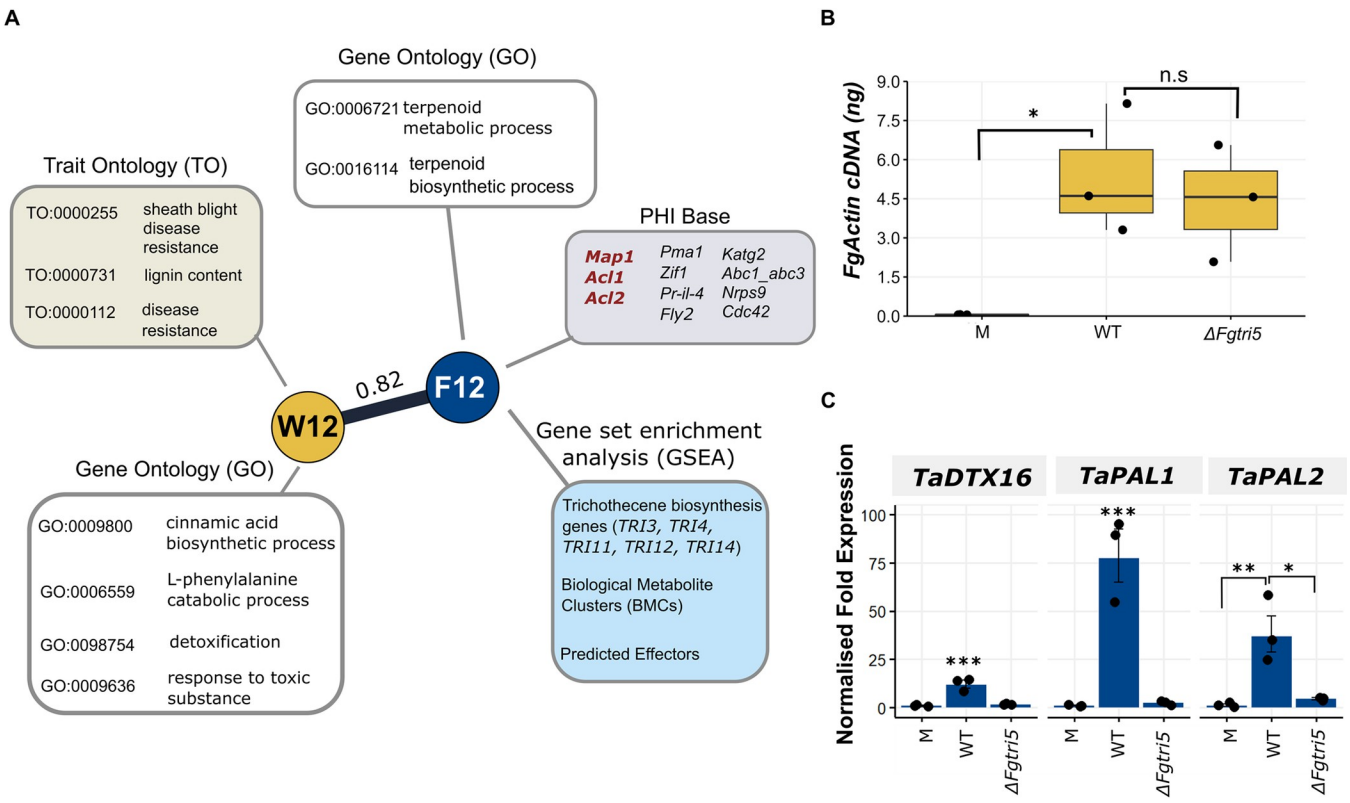

Fig 4. Validation of correlation between the trichothecene mycotoxin biosynthesis gene enriched module (F12) and the detoxification gene enriched module (W12). A. Modules F12 (N = 124) and W12 (N = 451) depicted with significant enrichment annotations and genes with known phenotypes from PHI-base. Three genes listed in red in the PHI-base annotation (grey box) exhibit a loss of pathogenicity phenotype, while the remaining genes display a reduced virulence phenotype when individually deleted in *F. graminearum*. **B.** Equal levels of fungal burden were observed in tissue samples ($p > 0.05$). Absolute quantity of actin cDNA in mock (M), *ΔFgtri5*, and wild-type (WT)-recovered from the base of the inoculated spikelet and RI1-2 tissue sampled at 3 dpi (N = 3). Significance was determined by a one-way ANOVA followed by Tukey HSD correction. **C.** Normalised fold change expression of selected W12 wheat genes in mock (M), *ΔFgtri5*, and WT-recovered base of the inoculated spikelet and RI1-2 tissue sampled at 3 dpi (N = 3). Significance is denoted as * = $p < 0.05$, ** = $p < 0.01$, and *** = $p < 0.001$. Significance was determined by a one-way ANOVA followed by Tukey HSD correction.

https://doi.org/10.1371/journal.ppat.1012769.g004

was examined (Fig 4A). This was achieved by inoculating wheat plants with either the wild-type *F. graminearum* reference strain PH-1 or the DON-deficient *ΔFgtri5* mutant strain, which was generated in the PH-1 background. Since *TRI5* is essential for DON biosynthesis, the primary function of the *TRI* gene cluster, the *ΔFgtri5* mutant effectively acts as a representation of the function of the entire cluster. Expression of three wheat genes was studied, including two phenylalanine ammonia-lyases (*PAL1* and *PAL2*; TraesCS4A02G401300 and TraesCS2D02G377200) which were annotated with the term disease resistance (TO:0000112), and a predicted transmembrane exporter, detoxification gene 16 (*DTX16*; TraesCS5B02G371100).

The base of the inoculated spikelet and first two rachis internodes below the point of inoculation (POI) were sampled at 3 days post inoculation (dpi). Levels of *FgActin* cDNA were not significantly different between treatments (Fig 4B). Expression of the three wheat genes from module W12 was significantly lower in the *ΔFgtri5* infected samples relative to wild-type infection (Fig 4C). This indicates that expression of genes in module W12 is correlated with DON production, thereby supporting the correlated co-expression patterns observed between modules of the two networks.

Dual co-expression networks as a tool to identify key genes necessary for virulence

To identify novel genes necessary for virulence, modules were examined for their potential biological importance based on their patterns of expression. Across the fungal modules, the module F16 is uniquely highly expressed during the earliest stages of infection, with markedly decreased expression at all the other stages of infection. Despite being highly expressed at a critical point for fungal establishment, the module has few characterised genes (6/76) and no significant enrichment annotation. This module is highly correlated to two wheat modules. These are W01 (R = 0.91; $p = 5 \times 10^{-7}$) and W05 (R = 0.85, $p = 2 \times 10^{-5}$). W01 is the largest wheat module and is enriched for defence response genes (GO:0006952; $p = 3.60 \times 10^{-08}$), but also maintenance genes which include photosynthesis (GO:0015979; $p = 4.59 \times 10^{-29}$) and RNA modification (GO:0009451; $p = 1.42 \times 10^{-47}$) GO terms. The wheat module W05 is enriched for disease resistance (TO:0000112, $p = 2.55 \times 10^{-178}$) and for the term oxidative stress (TO: 0002657; $p = 3.88 \times 10^{-34}$), suggesting that genes in the correlated fungal module F16 are possibly required for tolerance to this stress. Four genes in module F16 result in reduced virulence when individually deleted. These are *FgNPC1* (sterol trafficking) [42], *FgSrp2* (mRNA splicing) [45], and the transcription factors *GzCon7* and *Gzc2h045* [43] (**Table 1 and S2 File**). However, no gene deletion mutants exhibiting a loss of pathogenicity have yet been identified within this module, even though the eigengene expression pattern clearly indicates an association with the early establishment of the fungus in this key host tissue.

In WGCNA, genes with high module membership (MM) (i.e. intramodular connectivity) are predicted to be central to the biological functions of the module [30] and this continues to be a metric to identify biologically significant genes within WGCN analyses [58–60]. Following methods by Mateus et al. (2019) [39] key genes were defined as those exhibiting elevated MM within the module, which were also strongly correlated ($R > |0.70|$) with modules of the partner organism (wheat). In accordance with this, to identify genes in F16 that were likely necessary for virulence, the initial candidate gene list was selected by examining the 15 key genes with the highest MM from the 74 genes in the module (**S1 Table and S3 File**). Genes were then excluded that were likely to have functional redundancy (i.e. belonged to a gene family or had ancient paralogues within PH-1) to avoid compensatory effects when performing single gene deletion thereby leading to no changes in phenotypes (**S1 Table**). Ultimately, only two genes met these criteria: FGRAMPH1_01T23707 and FGRAMPH1_01T27545. FGRAMPH1_01T27545 has been previously characterised as the Niemann–Pick type C gene (*FgNPC1*). *FgNPC1* is necessary for sterol trafficking, with its deletion resulting in ergosterol accumulation within the vacuole and a reduced virulence upon wheat infection [42]. Orthologue analysis identified that the FGRAMPH1_01T23707 gene was a 1:1 orthologue of Killer-nine resistant 4 (Knr4) in *Saccharomyces cerevisiae* [61], therefore the orthologue in *F. graminearum* is henceforth referred to as *FgKnr4*.

FgKnr4, a key gene of module F16, is necessary for establishment of fungal infection

T. aestivum cv. Bobwhite was inoculated at anthesis with three independent *ΔFgknr4* transformants (**Fig 5A and 5B**), where *FgKnr4* was deleted using a split hygromycin replacement cassette (**S5A and S5B Fig**). No symptomatic disease progression past the inoculated spikelets was observed with each *ΔFgknr4* transformant (**Fig 5A and 5B**). While the inoculated spikelets developed symptoms, these did not exhibit full bleaching of the spikelet characteristic of FHB infection. Instead, eye-shaped lesions formed akin to those evident following *ΔFgtri5* mutant

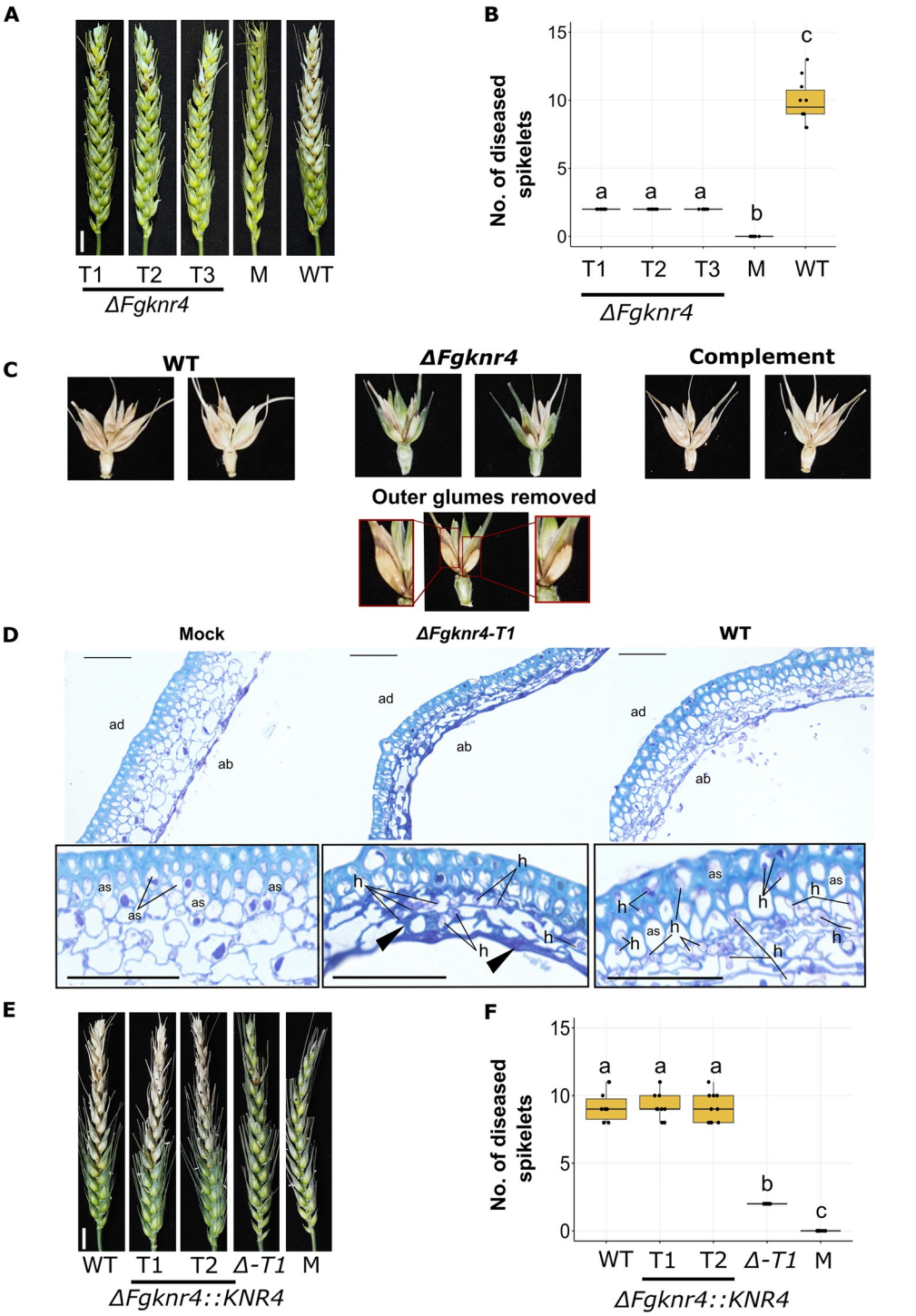

Fig 5. Decreased virulence observed during *in planta* infection with *ΔFgknr4*. A. Wheat spike infection assay done on the susceptible cultivar Bobwhite point inoculated with sterile water only (M), wild-type *F. graminearum* conidia, or conidia from three independent single gene deletion *F. graminearum* mutants lacking *Knr4* (*ΔFgknr4*, T1-3). Images were captured at 15 dpi. Scale bar = 1 cm. **B.** Number of diseased spikelets per wheat spike at 15 dpi (N = 10). Letters indicate significant differences (ANOVA, TukeyHSD $p < 0.05$). **C.** Symptom development on the inoculated spikelets and adjacent rachis tissues at 15 dpi. This includes an image of an *ΔFgknr4* inoculated spikelet with the outer glumes removed and zoomed in insets of the eye-shaped lesions. **D.** Ultra-thin 1 μm LR White resin sections stained with 0.1% Toluidine Blue for visualisation of wheat cell walls (light blue) and fungal hyphae (purple) of inoculated spikelet lemma tissue harvested at 7 dpi. Ab = abaxial wheat cell layer, ad = adaxial wheat cell layer, as = air spaces, and

h = fungal hyphae. In wheat inoculated with *ΔFgknr4* compared to WT, decreased host colonisation is observed, evidenced by (i) reduced fungal hyphae proliferation, particularly in the thicker adaxial cell layer, (ii) collapsed air spaces in wheat cells, and (iii) increased polymer deposition at the wheat cell walls (black arrows), indicating an enhanced defence response. Scale bar = 50 μm. **E.** Wheat spike infection complementation assay done on the susceptible cultivar Bobwhite treated with conidia either from wild-type *F. graminearum*, different complemented transformants (*ΔFgknr4*::*KNR4-T1* and *T2*), the single gene deletion mutant (*ΔFgknr4-T1*), or sterile water (M). Images were taken at 15 days post inoculation. **F.** Number of diseased spikelets per wheat spike at 15 dpi (N = 10). Letters indicate significant differences (ANOVA, TukeyHSD $p < 0.05$).

https://doi.org/10.1371/journal.ppat.1012769.g005

infection [52] (**Fig 5C**). Plating of surface sterilised wheat dissected into its constituent parts revealed the absence of fungal growth in un-inoculated spikelets (**S6 Fig**). Nevertheless, browning was noted in the rachis tissue immediately adjacent to the point inoculated spikelet, accompanied by fungal growth. However, this colonisation did not occur past the rachis internode of the 3rd spikelet. These data suggest that, despite entering the rachis, the *ΔFgknr4* mutant is unable to grow through the rachis node tissue and re-enter other spikelets. Microscopic examination revealed that while *ΔFgknr4* can colonise host tissue, it does so less effectively compared to the wild-type strain (**Fig 5D**). Despite highly reduced virulence, DON mycotoxin was detected in the inoculated spikelet and adjacent rachis internodes ($\geq$ 0.2 ppm). However, DON was undetectable in the neighbouring uninoculated spikelet ($<$ 0.2 ppm) (**S6B Fig**). Complementation of the mutant with wild-type *FgKnr4* (**S5C and S5D Fig**) restored virulence to wild-type levels (**Fig 5E and 5F**).

FgKnr4 influences cell wall structure, stress resistance, and growth

In vitro growth of *ΔFgknr4* was examined by culturing the fungus on both high or low nutrient agar. In both conditions a decreased growth rate relative to the wild-type was apparent (**Figs 6A and S7, S8**). In addition to this, conidia of *ΔFgknr4* appear smaller than wild-type (**S9A and S9B**). Despite these morphological differences *ΔFgknr4* retains the ability to produce perithecia and ascospores, albeit 8 days later than the wild-type (**S9C, S9D, S9E and S9F Fig**).

The *FgKnr4* (F16) module was correlated with the wheat module W05, which exhibits a significant enrichment in the term oxidative stress (TO: 0002657; $p = 3.88 \times 10^{-34}$) that encompasses a total of 1143 genes. Among these genes are two respiratory burst oxidase homologues (RBOH), specifically a predicted homolog of RBOF (TraesCS1A02G347700) and RBOHE (TraesCS5D02G222100), along with predicted catalase homologues, CAT3 (TraesCS7B02G473400) [62,63], and two CAT4 genes (TraesCS5B02G023300, TraesCS5D03G079400) [64]. This would suggest a necessity of a functional *FgKnr4* gene in oxidative stress tolerance that is critical during this early infection stage, where the fungus confronts various reactive oxygen species produced by the plant in response to fungal infection.

Stresses encountered by the fungus during *in planta* infection were mimicked *in vitro* using chemical stressors. As predicted by the correlation to wheat module W05, *ΔFgknr4* had increased susceptibility to oxidative stress (H_2O_2) (**Figs 6A, S7B, S7C and S8**). The *ΔFgknr4* mutant was also susceptible to other stresses faced during *in planta* infection including osmotic stress (1.5M NaCl), and calcofluor white induced cell wall damage compared to the wild-type and complemented strains (**Figs 6A, S7B, S7C and S8**). These susceptibilities may be due to changes in the cell wall structure of the *ΔFgknr4* strain. Corroborating this hypothesis, staining for chitin found an irregular deposition of chitin on the *ΔFgknr4* conidial cell wall, specifically at the tips and septa of the conidia (**Figs 6B and S10**). Furthermore, an irregular cell wall structure was observed upon transmission electron microscopy (TEM) analysis of the *ΔFgknr4* conidia, indicative of an abnormal cell wall composition (**Figs 6C and S11**).

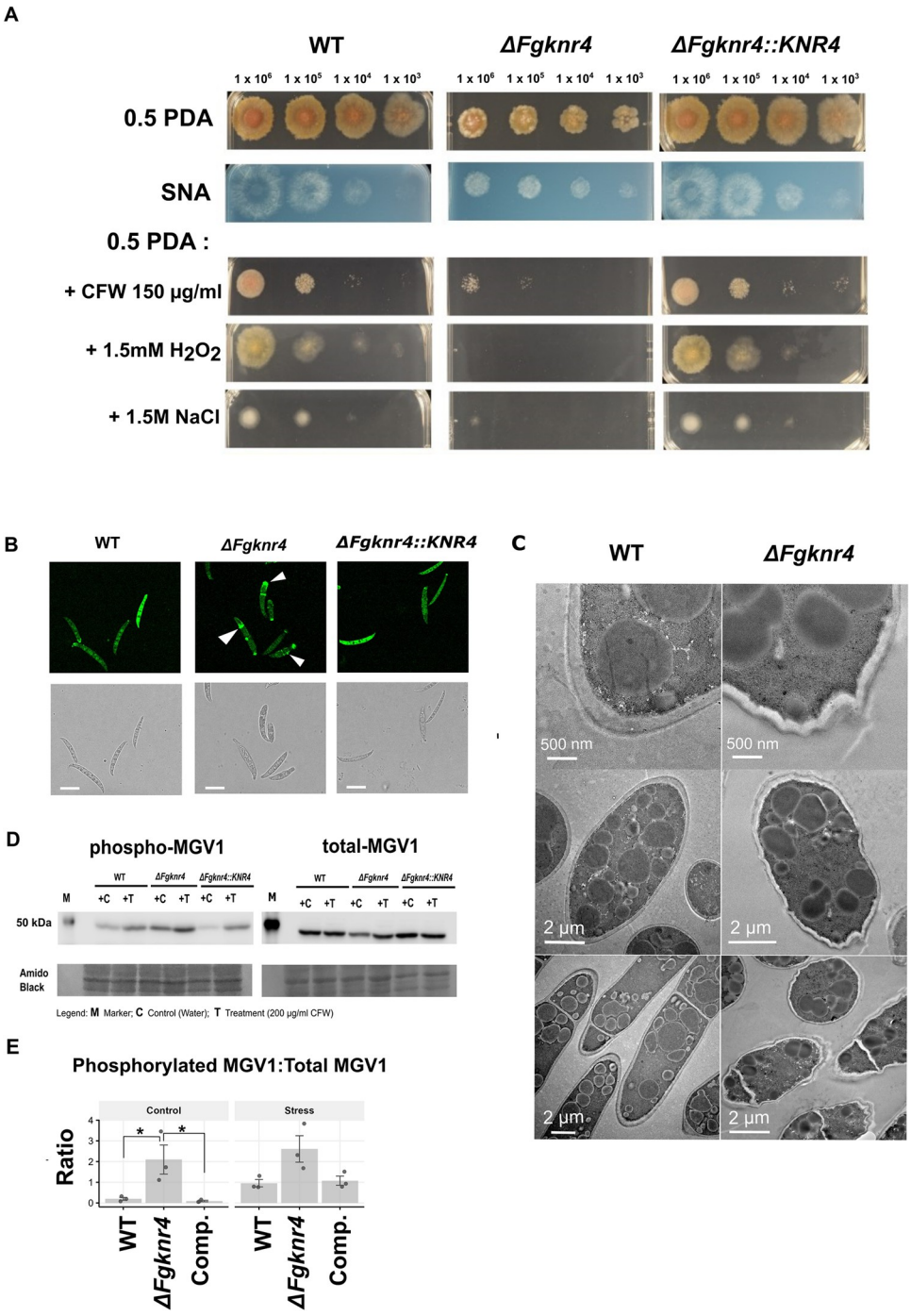

Fig 6. Cell wall stress sensitivity and abnormal cell wall morphology of *ΔFgknr4*. **A**. Dilution series of wild-type (WT), *ΔFgknr4*, and *ΔFgknr4*::*KNR4* strains on Synthetic Nutrient Agar (SNA) and half-strength Potato Dextrose Agar (0.5 PDA) with and without the addition of calcofluor white (CFW), hydrogen peroxide (H_2O_2), and sodium chloride (NaCl). The dilution series begins at 1 x 10^6 and continues with 10-fold dilutions. Images taken after 3 days of growth at room temperature. This experiment was replicated twice with similar results. **B**. Abnormal chitin deposition patterns in *ΔFgknr4* conidia. Chitin-stained in conidia visualised using Wheat Germ Agglutinin Alexa Fluor 488 Conjugate (WGA). Scale bar = 50 µm. **C**. TEM imaging of wild-type and *ΔFgknr4* conidia, showing differences in cell wall structure **D.** Western blot of proteins extracted from, *ΔFgknr4* and *ΔFgknr4*::*KNR4* mycelium incubated without (C) or with (T) the addition of 200 µg/ml calcofluor white (CFW) for 24 h. Phospho-p44/42 MAPK (Erk1/2) and p44/42 MAPK (Erk1/2) antibodies were used to detect phosphorylated and total MGV1, respectively. Amido black total protein staining was performed to compare protein loading. **E.** Ratio of phosphorylated MAPK/total MAPK based on

quantification of band intensity. Significance is denoted as * = $p \leq 0.05$. Significance was determined by a one-way ANOVA followed by Tukey HSD correction.

https://doi.org/10.1371/journal.ppat.1012769.g006

The involvement of *FgKnr4* in cell wall metabolism was further studied by examining its effect on the cell wall integrity pathway (CWI). The fungal CWI pathway is triggered in response to various stresses (e.g. oxidative stress, osmotic pressure, cell wall damage) [65] and in *F. graminearum* is activated through the phosphorylation of the MAP-kinase (MAPK) *FgMGV1* [66,67]. A Western blot was run on mycelium samples grown with and without a cell wall stress (calcofluor white). Constitutive activation of MGV1 in the absence of stress and increased phosphorylation under stress was observed in *ΔFgknr4* when compared to the wild-type (**Fig 6D and 6E**). This finding is consistent with previous observations in *S. cerevisiae* [68]. This reinforces the biological function of *FgKnr4*, suggesting an involvement in fungal stress responses and cell wall morphology in *F. graminearum*.

Although the module F16 lacked significant enrichment for ontology terms and unique gene sets, 8/15 of the candidate genes within the module were related to cell division and ATP binding genes through connections based on protein similarity and orthology (**S1 Table and S12 Fig**). Four of the candidate genes were also part of a predicted protein-protein interaction subnetwork of genes which relate to cell cycle and ATP binding within module F16 (**Fig 7A**). To determine if *FgKnr4* was involved in the cell cycle, as suggested by the shared genes in the module, the mutant was tested for susceptibility to benomyl, a microtubule inhibitor commonly used to identify mutations affecting cell division [69]. The *ΔFgknr4* mutant was more susceptible to benomyl than the wild-type and complemented strain, with a greater inhibition when grown both in liquid culture (**Fig 7B**) and in solid media (**Fig 7C**).

The orthologous gene in the wheat pathogen *Zymoseptoria tritici* is also important for cell wall integrity and virulence on wheat

Analysis of the Knr4 protein conservation found that orthologues were highly distributed across the Dikarya, occurring in both Ascomycota and Basidiomycota (**Fig 8**). Notably, no orthologues of the gene were found in other Eukaryotes or basal fungal lineages, highlighting its specificity to the lifestyle of the Dikarya. This high level of conservation across fungi suggests that phenotypes observed in *F. graminearum* may also be conserved in other economically significant pathogenic fungi.

The orthologous *Knr4* gene in another wheat fungal pathogen *Z. tritici* (*ZtKnr4*, Mycgr3G105330) was disrupted to test for conserved gene function. Despite the phylogenetic distance between the two fungi, the FgKnr4 and ZtKnr4 proteins share 43.5% pairwise identity. Alphafold3 was successfully used to accurately model the core region of the Knr4 protein, as evidenced by the high similarity between the predicted core structure of ScKnr4 and its X-ray crystal structure (**S13A and S13B Fig**). Structural predictions for both FgKnr4 and ZtKnr4 also revealed a strong similarity in their core regions, with a root-mean-square deviation (RMSD) of 1.060, indicating a high degree of structural conservation (**S13C, S13D and S13E Fig**).

Mirroring the phenotype observed in *F. graminearum*, reduced virulence (chlorosis but limited to no necrosis) was observed when wheat leaves were inoculated with *ΔZtknr4* (**Figs 9A and S14**). In addition to this the *ΔZtknr4* mutant was susceptible to calcofluor white induced cell wall stress and exhibited reduced hyphal branching (**Fig 9B and 9C**). These results highlight the potential of employing the *Fusarium*-wheat dual co-expression approach to gain insights into fungal-plant interactions, both within *Fusarium* species and across the fungal kingdom.

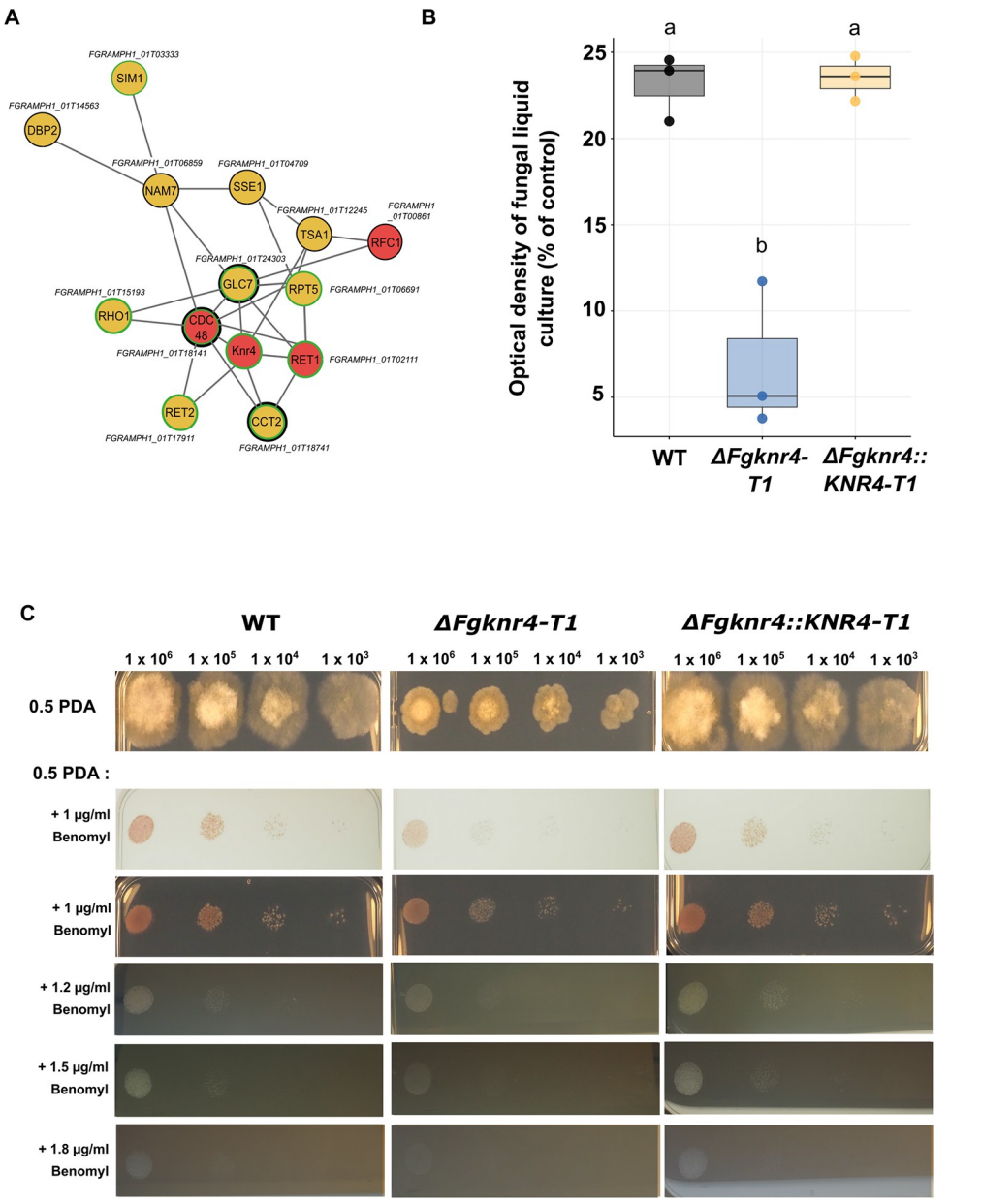

Fig 7. *FgKnr4* is associated with cell cycle genes and sensitive to the microtubule inhibitor benomyl. A. Protein-protein interaction subnetwork of *S. cerevisiae* orthologs of genes in module F16 relating to cell cycle and ATP binding. Each node is the BioGRID ID of an *S. cerevisiae* protein with each grey vertex representing a direct protein-protein interaction recorded on the database. The corresponding *F. graminearum* ID is provided next to each protein node. Red nodes indicate that this protein is an orthologue of a candidate gene from the F16 module. Black borders indicate proteins involved in ATP binding, while green borders denote proteins associated with cell cycle processes, as identified through Knetminer and/or BioGRID. **B.** Relative growth inhibition in Potato Dextrose Broth (PDB) containing 0.5 μM benomyl compared to growth in PDB without the stress. Cultures were inoculated with either wild-type (WT), *ΔFgknr4*, or *ΔFgknr4*::*KNR4*. Optical density readings were taken 48 hours post-inoculation. Each biological replicate (N = 3) consists of three technical replicates. Letters indicate significant differences (ANOVA, TukeyHSD $p < 0.01$) **C.** Dilution series of wild-type (WT), *ΔFgknr4*, and *ΔFgknr4*::*KNR4* strains on half-strength Potato Dextrose Agar (0.5 PDA) with and without the addition of benomyl. Images of plates treated with 1 μg/ml benomyl were captured on both a lightbox and a dark background. The lightbox images more clearly reveal the increased susceptibility of *ΔFgknr4*, which is obscured by the growth of aerial hyphae in the dark background images. The dilution series begins at 1 x 10^6 and continues with 10-fold dilutions. Images taken after 3 days of growth at room temperature.

https://doi.org/10.1371/journal.ppat.1012769.g007

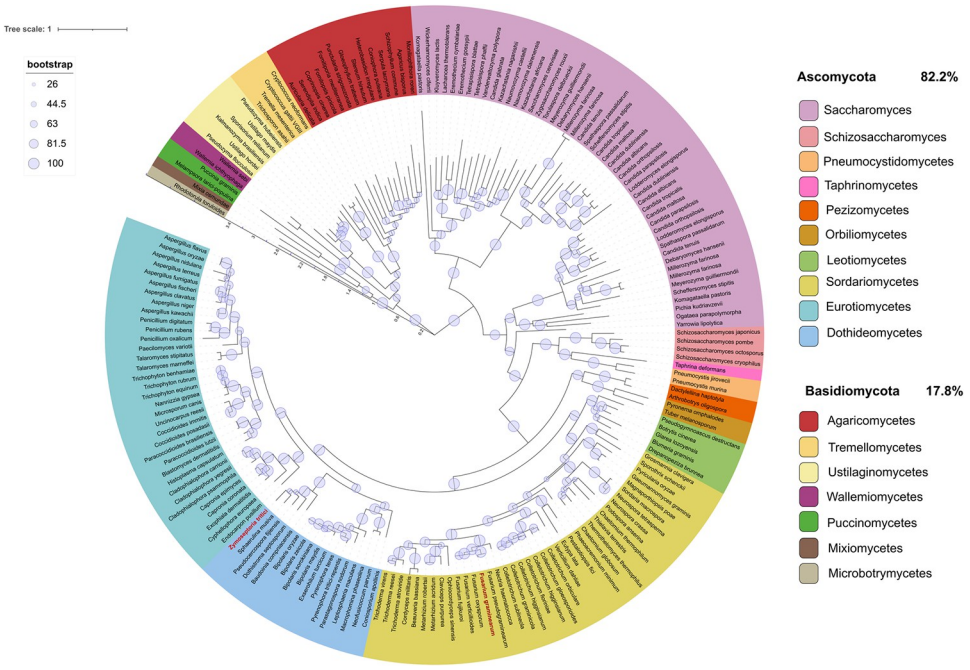

Fig 8. Distribution of Knr4 orthologues across eukaryotes reveals exclusive presence in fungi. A phylogenetic tree depicting the distribution of Knr4 orthologues across Eukaryota, with the positions of *F. graminearum* and *Z. tritici* highlighted in red. Different taxonomic levels are indicated in various colours as specified in the legend, alongside the percent distribution of orthologues between Ascomycota and Basidiomycota. Evolutionary distances between species or taxa are denoted by an internal scale (range 0–3.5). Bootstrapping confidence values are depicted as pale blue circles, with increasing size corresponding to higher confidence.

https://doi.org/10.1371/journal.ppat.1012769.g008

Discussion

The generated dual *F. graminearum*-wheat co-expression network was successfully used to identify a gene necessary for virulence. By analysing stage-specific modules of infection, module F16 was identified, which exhibited high gene expression levels during the symptomless stage of FHB infection and had no significant GO enrichment patterns but was correlated to a wheat module enriched for oxidative stress genes. Within module F16, the gene *FgKnr4* was found to have a high module membership score, indicating its central role in the module. Experimental validation showed that *FgKnr4* is essential for responding to chemical compounds that induce cell wall stress (including oxidative stress) and cell cycle inhibition, for early establishment of *in planta* infection, and for subsequent disease progression in wheat spikes. Similarly, the deletion of *Knr4* in another pathogenic species, namely *Z. tritici* resulted in a reduced virulence phenotype in leaves and displayed a comparable cell wall stress phenotype. This highlights the utility of pathogen-host co-expression network analysis in identifying conserved genes necessary for virulence across wheat fungal pathogens.

The predictions from the WGCNA were validated for the F12-W12 correlation through the experimental confirmation of the co-regulation of the *F. graminearum* trichothecene mycotoxin and wheat detoxification genes during infection. For *F. graminearum*, module F12 was of exceptionally high interest because of its positioning specifically at the transition between the late symptomless stage and the early symptomatic stage. For wheat genes in the correlated module W12, the studied genes included two phenylalanine ammonia-lyases (*PAL1* and *PAL2*) along with a predicted detoxifying efflux transporter (*TaDTX16*). Supporting these findings, previous transcriptomic studies on wheat spikes treated with or without DON have

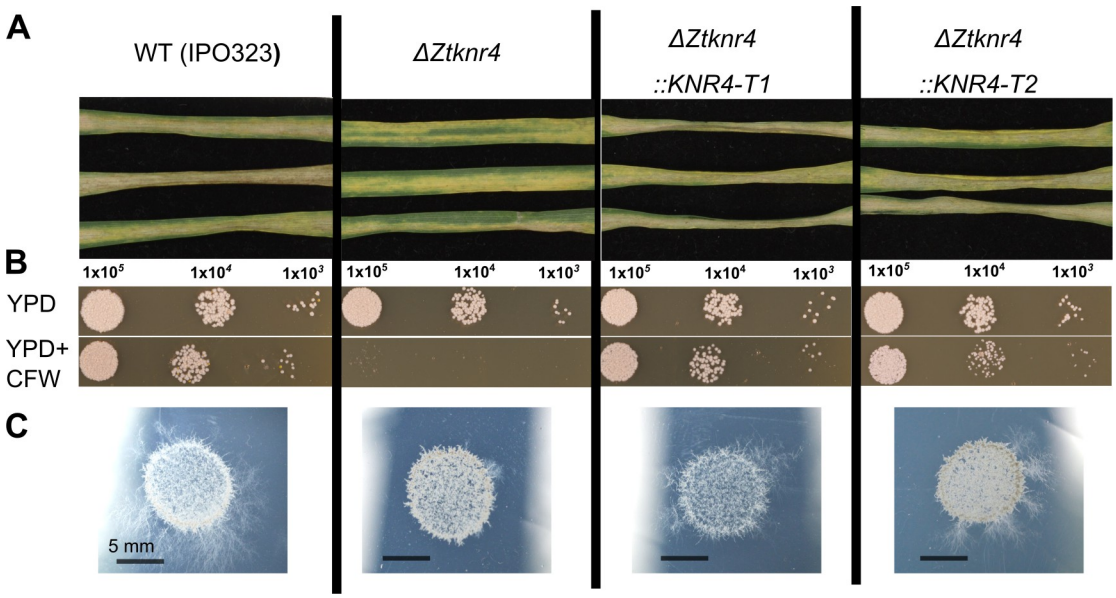

Fig 9. Functional characterisation of the *Zymoseptoria tritici ΔZtknr4* gene deletion mutant. A. Detached wheat leaves inoculated with wild-type (WT), *Z. tritici* (IPO323), *ΔZtknr4* mutant strain, and two complemented strains (*ΔZtknr4*::*KNR4-T1* and *T2*). Images taken at 20 dpi. **B.** WT *Z. tritici*, the *ΔZtknr4* mutant and two complemented strains (*ΔZtknr4*::*KNR4-T1* and *T2*) spot inoculated onto YPD agar with (bottom) and without (top) calcofluor white (CFW). Dilution series begins at 1 x 10^5 and continues with 10-fold dilutions. Images taken after 3 days of growth at room temperature (RT). **C.** WT *Z. tritici*, the *ΔZtknr4* mutant and two complemented strains (*ΔZtknr4*::*KNR4-T1* and *T2*) spot inoculated onto 1% Tap Water Agar (TWA). Images taken after 10 days of growth at room temperature (RT).

https://doi.org/10.1371/journal.ppat.1012769.g009

shown that these genes respond to DON exposure [70]. Specifically, *TaPAL1* and *TaPAL2* were expressed in a susceptible wheat cultivar treated with DON, while *TaDTX16* was expressed in a resistant cultivar carrying the Fhb1 resistance QTL upon DON treatment. This suggests that *TaDTX16* may also play a role in the Fhb1-mediated resistance response. Although *TaPAL1* and *TaPAL2* have not been previously studied for their direct involvement in disease resistance in the wheat—Fusarium interaction, the *PAL* gene family is known to be associated with disease resistance and other phenotypes [71]. In multiple plant species (including *Arabidopsis*, pepper (*Capsicum annuum)*, and rice (*Oryzae sativa)*), *PAL* is induced in response to biotic and abiotic stresses, which includes pathogen induced stress [72–75], and in numerous genetically incompatible host-pathogen interactions mediated by cognate R-Avr proteins including responses to fungi [76,77]. *TaDTX16* is part of the multidrug and toxic compound extrusion (*MATE*) gene family and was named after its orthologue in *Arabidopsis thaliana* [78]. *DTX/MATE* genes take part in heavy metal and lethal compound detoxification in plants and could be involved in mycotoxin detoxification [79]. Previously, a wheat *DTX* gene was reported to be highly expressed in resistant cultivars of wheat compared to a susceptible wheat cultivar when infected with *F. graminearum* [36]. Furthermore, *TaDTX16* is located on chromosome 5BL within an interval harbouring a resistance QTL for defence against the necrotrophic fungal disease Septoria nodorum blotch [80]. While these *ΔFgtri5* responsive genes have been identified, wheat genes were not characterised from the network due to several challenges including limitations from mapping genes to the Chinese Spring reference genome, genetic redundancy due to homoeologous genes and large gene families, and the presence of DON, which can inhibit translation and prevent many transcriptional changes from being realised within the host responses.

The characterisation of *FgKnr4*, underscores the importance of identifying genes necessary for full virulence through gene expression studies. This approach is essential because predicting the pathogenic potential of Fusarium species based solely on comparative genomics is challenging due to the absence of significant differences in secreted effector proteins, carbohydrate-active enzymes, or gene repertoires between pathogenic and endophytic strains of Fusarium and Fusarioid species [81]. *FgKnr4* was investigated further for its multifaceted roles in growth, stress response, and cell wall integrity. Supporting previous findings in *Fusarium asiaticum* [82], this study demonstrates that *FgKnr4* is involved in regulating growth rate, conidial spore morphology, and sensitivity to osmotic and oxidative stresses, and is necessary for full virulence and cell wall stress tolerance in *F. graminearum*. Moreover, this study establishes that Knr4 influences the well-studied cytoplasmically located Mgv1 cell wall integrity (CWI) MAPK pathway [83], resulting in visible abnormalities of the conidial cell wall **(Figs 6B, 6C, S10 and S11)**. The cell wall integrity pathway in *F. graminearum* is well-characterised, with each MAP-kinase in the cascade having been identified, studied, and shown to have roles in virulence reduction and/or asexual and sexual spore formation [66,84–86]. However, *FgKnr4* is not co-expressed with the MAP kinases it regulates. Among the MAP kinases, *FgMGV1* is found in module F13, which is consistently expressed throughout the infection process, reflecting the common pattern of MAPKs being primarily regulated post-transcriptionally. The other two MAP kinases, Bck1 and Mkk1, are part of module F05, which includes two chitin synthases—*FgChs3b* (FGRAMPH1_01T07327) [87] and FGRAMPH1_01T04707 (uncharacterised), as well as the glucan synthase *FgGls* (FGRAMPH1_01T26047) [88]. This module is highly expressed during the late symptomless phase (**S3 Fig**). In *S. cerevisiae*, ScKnr4 is found to be a scaffolding protein [89]. Given this, *FgKnr4* may be expressed earlier than the other members of the CWI pathway to prepare and scaffold regulatory signals between different signalling cascades. Our findings therefore reveal an additional layer of control within the *F. graminearum* cell wall integrity pathway mediated by *FgKnr4*. This discovery contributes to and further improves our understanding of the regulatory mechanisms governing cell wall integrity in *F. graminearum*. This new finding also offers the first insights into the regulatory effects of Knr4 in a filamentous fungus. This additional knowledge aids the development of novel strategies to mitigate losses caused by FHB disease and DON contamination.

Z. tritici possesses one of the most expansive publicly available eukaryotic pangenomes, with approximately 42% of its genes categorised as accessory [90]. *ZtKnr4* is part of the core *Z. tritici* genome of the European pangenome [91] and designated within the core orthogroup OG0008320 within the global (Europe, Asia, North and South America, Australia, and Africa) pangenome [92]. Given the highly variable nature of accessory chromosomes in *Z. tritici*, the assignment of *ZtKnr4* to the core genome in two separate pangenomic analyses underscores its importance in fungal physiology. *ZtKnr4* is also expressed throughout the wheat infection process [93]. Disruption of the gene resulting in a reduced virulence phenotype reinforces the potential of *ZtKnr4* as a candidate target for fungicide development, emphasising its significance in combating *Z. tritici* infections and mitigating agricultural losses. Despite the ever present global importance of STB disease for many decades [3,94] *Z. tritici* has far fewer functionally characterised genes, with only 99 genes with a characterised phenotype within the Pathogen Host-Interactions database and only 50 of these genes associated with a loss in pathogenicity or reduced virulence (http://www.phi-base.org/) [95,96]. The reduction in virulence observed in the *ZtKnr4* mutant therefore marks a valuable contribution to the characterisation of one of the >9000 core genes across the known *Z. tritici* pangenomes [91,92].

The high conservation and exclusivity of *Knr4* within the fungal kingdom, combined with its absence in other eukaryotes and its conserved function across related species, suggest that *Knr4* could be an ideal target for intervention. This could be achieved through the

development of chemical fungicides that disrupt the protein's function [97] or through the application of RNA interference techniques [98–100]. Stricter EU regulation of chemicals suitable for fungicide use in agricultural, medical and/or veterinary settings [101], combined with significant losses in fungicide efficacy due to the evolution of pathogen populations means there is a pressing need to identify new target sites for control. Therefore, this research not only advances our understanding of mechanisms required for full fungal virulence but also offers promising directions for the development of effective strategies for disease control in agriculture.

Materials and methods

Gene co-expression network analysis

RNA-seq reads from Dilks et al. (2019) [31] were provided by Dr Neil Brown (European Nucleotide Archive: PRJEB75530). Read quality was assessed with FastQC v. 0.11.9 (Andrews, 2010, [102] https://www.bioinformatics.babraham.ac.uk/projects/fastqc/). Reads were mapped to a combined Fusarium–wheat genome, consisting of v. 5 of the *Fusarium graminearum* PH-1 genome [103] and the high confidence (HC) transcripts of the v. 2.1 of the International Wheat Genome Sequencing Consortium (IWGSC) *Triticum aestivum* genome cultivar Chinese Spring [104]. Genome indexing and read alignment were performed using STAR aligner 2.7.8a [105]. Soft clipping was turned off to prevent reads incorrectly mapping to similar regions of the highly duplicated hexaploid wheat genome. Reads were filtered using the filterByExpr function part of the R package Edge R v.3.32.1 [106]. Fragments Per Kilobase per Million mapped fragments (FPKM) was calculated using the GenomicFeatures v.1.50.4 R package [107]. For the WGCN analysis raw counts were normalised separately for fungal and wheat reads by performing a variance stabilising transformation (VST) using the DESeq2 v 1.30.1 R package [108] in R (v4.0. 2, https://www.r-project.org/).

The VST normalised counts were filtered to remove any excessive missing values using the function goodSamplesGenesMS in the WGCNA R package [30]. Standard methods were implemented to generate the network using the WGCNA R package, with the following parameters. A signed-hybrid network was constructed using the filtered counts. The soft thresholding power (β) was uniquely selected per network according to scale free model criteria [40], where β = 9 for the fungal network and β = 18 for the wheat network (**S2 Fig**). A deepSplit of 3 was paired with a standard cutheight of 0.25. A minimum module size of 50 was selected to minimise potential transcriptional noise when assigning modules using smaller datasets [109,110]. The function multiSetMEs from the WGCNA package was used to calculate module eigengene expression. Module eigengenes with similar expression profiles were then merged.

Module quality and preservation was calculated using the function modulePreservation present in the WGCNA R package [30,41]. When calculating module preservation, the original wheat or fungal network was considered the reference network. Then 50 different test networks were created, each built upon randomly resampling (with replacement) a proportion of samples from the original dataset. The average preservation metrics (i.e. Z-score) between the original network and the 50 test networks was calculated for both the fungal and wheat networks.

Module enrichment an annotation

Gene ontology (GO) annotations of the v. 5 PH-1 genome (GCA_900044135.1) were generated using Blast2GO v .5 [111]. Enrichment was calculated using a background set of all genes present in the fungal network. GO annotations for the IWGSC v.2.1 genome were generated

by performing a BLASTx search on the NCBI nb database using DIAMOND v 2.0.13-GCC-11.2.0 [112], then Blast2GO v.5 was used to annotate the BLAST hits with GO terms. GO term enrichment was calculated for each high level GO ontology (Biological Process, Molecular Function and Cellular Component) using the R package topGO v 2.46.0 [113].

Plant Trait Ontology (TO) [114] enrichment analysis was performed using gene-trait annotations derived from the KnetMiner knowledge graph (release 51) for wheat [115] and KnetMiner notebooks available at: https://github.com/Rothamsted/knetgraphs-gene-traits/. Predicted effectors were determined using EffectorP v.3.0 [116]. Alongside this, predictions to identify extracellularly localised proteins were done using SignalP v6.0 [117]. Custom *F. graminearum* gene set enrichment of the network modules was calculated by performing a Fisher's exact test using all the genes in the fungal network as the background gene set. A Benjamini-Hochberg (BH) correction was calculated for both GO and custom enrichments [118]. Modules were deemed significantly enriched if $P\text{-}corr < 0.05$.

Gene lists included in the Gene Set Enrichment Analysis (GSEA) consisted of predicted secreted effector proteins, alongside known gene families associated with virulence, such as biological metabolite clusters (BMCs) [119], polyketide synthases [120], protein kinases [121] and transcription factors [43]. Due to their well-established importance in *F. graminearum* pathology, a separate enrichment for genes of the *TRI* gene cluster was also performed.

Annotation from PHI-base was obtained by mapping genes to version PHI-base (v4.16) annotation using UniProt gene IDs and any through Decypher Tera-Blast P (TimeLogic, Inc. Carlsbad, California, USA) (E-value = 0) against the PHI-base (v4.16) BLAST database [95,96].

The Knetminer network of F16 key genes was generated by providing all 15 key genes as input in the web interface of *Fusarium graminearum* Knetminer version 51 (https://knetminer.com/Fusarium_graminearum/). The protein-protein interaction subnetwork was created by using Orthologous Matrix (OMA) [122] to identify orthologues of *F. graminearum* in *S. cerevisae*. This was then used to map orthologues to *S. cerevisae* protein-protein interactions on BioGRID version 4.4.236 [123].

Fungal material and growth conditions

F. graminearum strains were cultured and conidia prepared as previously described [12]. Fungal strains were grown in the dark for 3 days on nutrient-rich potato dextrose agar (PDA), nutrient-poor synthetic nutrient agar (SNA; 0.1% KH_2PO_4, 0.1% KNO_3, 0.1% $MgSO_4 \cdot 7H_2O$, 0.05% KCL, 0.02% glucose, 0.02% sucrose and 2% agar) and PDA with different cell wall stresses. This included 1–1.8 μg/ml benomyl, 150/100 μg/ml calcofluor white, 1.5mM H_2O_2, and 1.5M NaCl. Plates were point inoculated with 20 μl of 4-fold dilution series starting with 1 x 10^6 conidia/ml. For growth rate inhibition calculations, plates were point inoculated with 20 μl 1 x 10^6 conidia/ml water suspensions. Colony diameter was measured at 3d growth and relative inhibition was calculated as (colony diameter in 0.5 PDA with stress)/(colony diameter in 0.5 PDA without stress) for each strain. Sensitivity to benomyl in liquid cultures was tested by mixing 100 μl of 1 x 10^5 conidia/ml or 100 μl water (control) with 100 μl of Potato Dextrose Broth (PDB) without and with 0.5 μM benomyl in a 96 well plate incubated at 22 ℃ and 118 rpm for 48 hrs. Optical density (OD) was measured at 600 nm and the readings of fungal inoculated cultures were corrected by subtracting readings from corresponding control wells.

For the growth rate assay, fungi were grown on PDA and measurements were taken after 3, 5, and 7 days. Surface sterilisation of wheat spikes was performed by submerging single wheat spikelets in 1/8 diluted thin bleach for 3 min, followed by three washes with sterile distilled H_2O. Dissection was done using a razor blade to separate the point inoculated spikelets and adjacent spikelets (**S6A Fig**). Wheat tissue was placed on SNA and images were taken after a

3-day incubation at room temperature in the dark. Perithecia induction was achieved as described in Cavinder et al. (2019) [124]. All plate images were taken using an Olympus OM-D camera with a 60mm ED M.Zuiko macro lens. Conidia and ascospore images were taken using the Axiomager 2 (Zeiss, Oberkochen, Germany) under brightfield illumination. Conidia lengths (N = 50) and perithecia heights (N = 40) were measured using ImageJ [125].

Fusarium graminearum genetic manipulations

The *FgKnr4* gene was deleted through split marker-mediated transformation to target fungal gene replacement with the hygromycin resistance cassette by homologous recombination [126]. *F. graminearum* gene deletion construct assembly and fungal transformation was performed following methods outlined in King et al., 2017 [127]. Primers were designed for the fusion of the 5' and 3' constructs using the NEBbuilder Assembly Tool v.1 (https://nebuilderv1.neb.com/). Using the Gibson Master Mix (New England Biolabs, UK) the paired split marker fragments were ligated into the pGEM—T Easy Vector (Promega, UK) then transformed into DH5α competent *Escherichia coli* (C2987H, New England Biolabs, UK) following the standard manufacturer protocol. Diagnostic PCRs were done using DreamTaq polymerase (ThermoFisher, UK) and standard cycling conditions. For the single gene deletion, in three separate transformants two diagnostic PCRs were done to detect the presence of the replacement cassette flanks (P3-4, P5-6) and the absence of the wild-type gene (P1-2) (**S5A and S5B Fig**). Complementation was performed following the protocol developed by Darino et al. (2024) [128]. Diagnostic PCRs for the complemented strains involved amplification of the insertion cassette flanks (P7-8; P1-9), testing for the absence of the short 868 bp empty intragenic locus amplicon (P11-P12), and testing for the heterozygosity of the geneticin gene (P13-P14) (**S5C and S5D Fig**). A full primer list is available in **S4 File**.

Wheat host inoculation

The susceptible spring wheat (*T. aestivum*) cultivar, Bobwhite, was grown to anthesis. The 5th and 6th spikelets from the top of the wheat spike were inoculated on both sides using 5 μl of 5 x 10^5 conidia/ml. Each treatment included 10 separate wheat plants (N = 10). After inoculation, plants were kept in a high humidity chamber for 48 h in the dark. Disease progression was documented every two days by scoring the number of bleached spikelets. At 15 dpi wheat spikelet tissue and the adjacent rachis internode was separated, frozen in liquid nitrogen, and ground to form a fine powder. The presence of DON mycotoxin was assessed using the Deoxynivalenol (DON) Plate Kit (Cat. 20–0016, Beacon Analytical Systems Inc., USA) following standard protocol. This experiment was replicated with three biological replicates per treatment (N = 3). All *F. graminearum* infected plant images were taken using an Olympus OM-D camera using a 60mm ED M.Zuiko macro lens.

For resin dissection microscopy wheat cv. Bobwhite was inoculated at the 7th and 8th true spikelets from the base on both sides using 5 μl 5x10^5 conidia/ml. After inoculation, plants were kept in a high humidity chamber for 48 h in the dark. Lemma tissues were excised from infected spikelets at 7 dpi, fixed in a 4% paraformaldehyde, 2.5% glutaraldehyde solution with 0.05M Sorensen's phosphate buffer (NaH_2PO_4:Na_2HPO_4, pH 7.0). Samples then underwent 3 further buffer washes, a subsequent ethanol dehydration protocol (0–100% EtOH) over 48hrs and then LR White resin (TAAB, Laboratories Equipment Ltd, UK) infiltration diluted with dry ethanol at increasing ratios (1:4, 2:3, 3:2, 4:1, 100%). Samples were inserted into capsules (TAAB, Laboratories Equipment Ltd, UK) and resin polymerised at 60˚C for 16 hours in a nitrogen oven (TAAB, Laboratories Equipment Ltd, UK). Ultra-thin 1 μm sections of samples were cut on an ultramicrotome (Reichert-Jung, Ultracut) with glass knives, placed onto glass

polysine slides (Sigma Aldrich, UK), dried at 70˚C, stained with 0.1% (w/v) Toluidine Blue O and mounted in DPX mounting medium (Fisher Scientific). Stained sections were imaged on a Zeiss Axioimager (Axiocam 512 color, Zeiss, Jena, Germany) light microscope with bright-field illumination.

Gene expression of module W12 genes

Bobwhite wheat plants were point inoculated at anthesis with either wild-type PH-1, *ΔFgtri5* or water only (Mock) following the protocol outlined in Dilks et al., (2019) [31]. Each experimental condition was replicated in triplicate, with each replicate deriving from three pooled independent wheat spikes. Tissues from the base of the inoculated spikelet and rachis internodes 1 and 2 were sampled and frozen in liquid nitrogen at 3 dpi. Sampling at this timepoint captures the early colonisation of the initially inoculated spikelet, where the macroscopic disease progression of *ΔFgtri5* is comparable to the wild type. Frozen samples were ground and RNA was extracted using the Monarch Total RNA Miniprep Kit (NEB, UK). Equal amounts of RNA were used to synthesise cDNA with Revertaid cDNA synthesis kit (ThermoScientific, UK). PowerTrack SYBR Green Master Mix (ThermoScientific, UK) was used for qPCR. To quantify fungal burden, cDNA was used instead of genomic DNA, as the entire tissue sample was required to generate cDNA. Consequently, the housekeeping gene *FgActin* was selected as a reference for quantifying fungal burden. Each biological replicate included three technical replicates. All primers are provided in **S4 File**.

Western blot

A 200 μl aliquot of a *F. graminearum* conidia solution (1 x 10^6 conidia/ml) was added to 10 ml potato dextrose broth (PDB) at 27˚C. Calcofluor white was added to a concentration of 200 μg/ml after 24 h of incubation at 180 rpm. Twenty-four hours after the addition of the stress, mycelium was harvested, flash frozen and freeze dried. To lyse the samples Y-PER Yeast Protein Extraction Reagent (ThermoScientific, UK) was added to the freeze-dried samples at 1.5 ml per 150 mg tissue, alongside Protease Inhibitor Cocktail (100x) (ThermoScientific, UK). Samples were lysed using the FastPrep-24 machine for 20s (MP Biomedical, USA). The supernatant was mixed with 5xSDS loading buffer (National Diagnostics, USA).

Equal amounts of protein (60 μg) were resolved on 8% SDS-PAGE gels (Mini-PROTEAN, Bio-Rad, UK) and transferred onto a nitrocellulose membrane. Immunoblots were performed by standard procedures using the Phospho-p44/42 MAPK (Erk1/2) (cat. #4370) and p44/42 MAPK (Erk1/2) (cat. #9102S) (Cell Signalling Technologies, USA) antibodies at their specified dilutions. The blots were developed using ECL Plus Western Blotting Detection Kit and images were acquired using Odyssey Imaging System (LI-COR Biosciences Ltd, Cambridge, UK).

Microscopic examination of cell walls

To induce conidia formation, 200 μl of frozen conidia (1 x 10^6) were plated onto PDA plates and the plates were incubated at room temperature under constant illumination. For conventional transmission electron microscopy (TEM), fresh conidia were harvested the same day from the PDA plates and pellets were fixed in a mixture of 2.5% glutaraldehyde and 4% Paraformaldehyde in Sorenson's buffer (SB) at pH 7.2 overnight at 4˚C. The samples were rinsed in SB and post fixed in 1% osmium tetroxide for 60 min at room temperature. The samples were dehydrated for 10 min per step into increasing concentrations of alcohol (30%, 50%, 70%, 90% and final 100%×3). Subsequently, the pure ethanol was replaced with propylene oxide, and the specimens were infiltrated with increasing concentrations (25%, 50%, 75%, and

100%) of Spurr resin mixed with propylene oxide for a minimum of 2 hr per step. The samples were embedded in pure, fresh Spurr resin and polymerised at 60˚C for 24 hr. Ultrathin sections (70 nm) were cut using an ultramicrotome (Leica UC7, Germany) and post-stained, first with Uranyless (TAAB Laboratories Equipment Ltd, UK) for 1 min and then with Reynolds lead citrate (TAAB Laboratories Equipment Ltd, UK) for 2 min at room temperature, prior to observation using a Transmission Electron Microscope (Jeol 2100plus, UK) operated at 200 kV.

F. graminearum conidia solution (1 x 10^6 conidia/ml) was stained with Wheat Germ Agglutinin, Alexa Fluor 488 Conjugate (WGA) (10 μg/ml) for 10 minutes each. Samples were washed three times in sterile distilled water after staining. A ZEISS 780 Confocal Laser Scanning Microscope (ZEISS, Germany) was used to image conidia.

Phylogenetic tree construction

Eggnogmapper-v5 [129] was used to map *FgKnr4* to the eggnog Orthologue Group (OG) ENOG502QTAZ and generate the phylogenetic tree. The tree was visualised and annotated using the interactive Tree of Life (iTOL) software [130].

Functional characterisation of the *Knr4* orthologue in *Z. tritici*

Separate analyses using BLASTp (E value = 3.7 x 10^{-110}) [131], Orthologous Matrix (OMA) [122], and Eggnogmapper [129] identified a single orthologous sequence in the genome of the *Z. tritici* isolate IPO323 (https://fungi.ensembl.org/Zymoseptoria_tritici/Info/Index) [14]. The gene has a Rothamsted gene model Id of ZtritIPO323_04g12347 [127,91] and is present on Chromosome 8 at start position 230142 bp. This maps to Mycgr3P105330 in the current genome call on Joint Genome Institute (JGI) Mycocosm [14]. Predicted folded protein structures and confidence plots were generated used the Alphafold3 server [132] (https://alphafoldserver.com/). The core X-Ray structure of ScKnr4 was downloaded from the RCSB Protein Data Bank (accession: 5J1B). Alignment between the ScKnr4 crystal structure and Alphafold3 predicted structure was done using the Pymol v.3.0.3 align function.

Agrobacterium-mediated fungal transformation [133] was performed to generate a series of independent gene disruption mutants of *ZtKnr4*. Flanking sequences and the hygromycin resistance gene were amplified from either genomic DNA or from plasmid pCHYG and using Phusion polymerase (NEB, UK). Fragments were gel purified using QIAquick Gel Extraction Kit (QIAGEN, UK) and assembled into the backbone (Kpn1 and BamH1 digested) of pCHYG by Gibson Assembly (NEB, UK). The resulting plasmids were transformed into the Agrobacterium strain AgL1 and fungal transformation of isolate IPO323 was performed as per standard protocols [133]. Positive transformants containing a disrupted *ZtKnr4* gene were identified by diagnostic PCR (**S15 Fig**). Complementation of the validated *ZtKnr4* mutant was performed through Agrobacterium-mediated transformation with plasmid pCGEN (digested EcoR1 and Kpn1) containing the native gene plus 1 kb upstream (5') and 300 bp (3') downstream genomic DNA, amplified by Phusion PCR (NEB, UK).

Attached leaf virulence assays were performed as per standard protocols [134] on wheat cultivar Riband. Leaf blades (N = 3) were inoculated with spore suspensions of 1 x 10^6 spores / ml in sterile water + 0.05% v:v Tween 20. Final disease assessments were made 20 days after inoculation. *In vitro* hyphal growth assays were performed following droplet inoculation of spore suspensions onto 1% Tap Water Agar (TWA) plates. Hyphal growth morphologies were determined by light microscopy and / or photography 10 days after inoculation. Calcofluor white sensitivity assays were performed to ascertain changes in cell wall strength. For this, spore suspensions were inoculated onto YPD agar (Formedium, UK) plates (control) and onto

YPD agar plates containing 200 μg / ml calcofluor white. Plates were incubated at RT for 8 days and then growth was monitored and recorded by photography. Images of *ZtKnr4 in planta* and *in vitro* experiments were taken with a Nikon D3200 camera. Disease levels were quantified using LemnaGrid image analysis system, as described in Chen et al. (2023) [91].

Supporting information

S1 Fig. Network Summary. A. Summary of all modules in the wheat network, including module size (number of genes), Gene Ontology (GO) and Trait Ontology (TO) enrichment summaries. **B.** Summary of all modules in the fungal network, including modules size, Gene Ontology (GO) enrichment summaries and Gene Set Enrichment Analysis (GSEA). Light blue indicates significant enrichment ($p < 0.05$) for the given term. The number of genes with different phenotypes in PHI-base are depicted, with LOP, RV, L and U denoting different PHI-base phenotypes (LOP = Loss of pathogenicity; RV = Reduced virulence; L = Lethal; U = Unaffected pathogenicity) (Urban et al., 2022) [95].
(TIF)

S2 Fig. Network statistics. A. Strength of correlation of network model (R-squared value) to scale free model at different soft thresholding powers. Dotted red line is at an R-squared value of 0.80, the threshold needed for generating a WGCNA network. **B.** Mean connectivity of genes in each network at different soft thresholding powers. A low mean connectivity is desired to meet the scale free network criteria. **C.** Module quality across all modules as determined by a Z-score calculation. Solid red lines at minimum quality (Z = 2) and high quality scores (Z = 10). **D.** Module preservation as determined by Z-score calculation against 50 random test networks. Solid red lines at minimum preservation (Z = 2) and high preservation scores (Z = 10).
(TIF)

S3 Fig. Summarised eigengene expression of all modules. Eigengene summarised expression plots illustrating the expression patterns of genes in **A Fungal** and **B Wheat** modules across different stages namely spikelet tissue (SP) at 3 and 7 dpi and A = Late symptomatic, B = Early symptomatic, C = Late symptomless, and D = Early symptomless.
(TIF)

S4 Fig. Annotation of stage-specific modules. Fungal modules (F) and wheat modules (W) depicted with significant enrichment annotations. Fungal modules are additionally annotated with known phenotypes from PHI-base. Genes listed in red in the PHI-base annotation (grey box) exhibit a loss of pathogenicity phenotype when deleted, while the remaining genes display a reduced virulence phenotype when deleted. Plots are separated by modules with highest expression in a given stage of infection, namely **A. Early symptomless, B. Early symptomless and late symptomatic, C. Late symptomless/Early symptomatic, and D. Late symptomatic.**
(TIF)

S5 Fig. PCR validation of single gene deletion and complementation of *FgKnr4*. A. Schematic for the hygromycin split marker deletion strategy including diagnostic primer locations (P1-6). **B.** Diagnostic PCR with primer sets depicted in panel A. PCR samples were separated on 0.75% agarose gel with a 1 kb DNA ladder. The expected amplicon size is given below the corresponding gel image. **C.** Schematic of gene complementation into the *Fg* transformation locus (Darino et al. 2024) [128], including diagnostic primer locations. **D.** Diagnostic PCR with primer sets depicted in panel C. PCR samples were separated on 0.75% agarose gel with a

1 kb DNA ladder. Expected amplicon sizes are written below the corresponding gel image.
(TIF)

S6 Fig. Surface sterilisation and DON quantification of dissected wheat floral tissue. A. Dissection of wheat spikes followed by separation of infected wheat spikelet and rachis tissues and subsequent plating onto synthetic nutrient agar (SNA) separated at 15 dpi. Plate images taken 3 days later. **B.** ELISA based quantification of DON in dissected spikelet (SP) samples of wheat inoculated with wild-type (PH-1) and *ΔFgknr4* at 15 dpi. Quantity of DON is measured in parts per million (ppm) and the detection threshold of the kit is indicated by a red line (ppm = 0.2). This experiment was replicated using tissue from three separate wheat spikes (N = 3).
(TIF)

S7 Fig. Characterisation of additional single deletion mutant and complemented *FgKnr4* transformants. A. Mean colony diameter of wild-type (WT), *ΔFgknr4*, and *ΔFgknr4*::*KNR4* grown on Potato Dextrose Agar (PDA) (N = 5). **B.** Dilution series of WT and additional *ΔFgknr4* transformants (*T2* and *T3*) on Synthetic Nutrient Agar (SNA) and half-strength Potato Dextrose Agar (0.5 PDA) with and without the addition of single stresses. **C.** Dilution series of WT and additional *ΔFgknr4*::*KNR4* transformants (*T2* and *T3*) on Synthetic Nutrient Agar (SNA) and half-strength Potato Dextrose Agar (0.5 PDA) with and without the addition of single stresses. The dilution series begins at 1 x 10^6 and continues with 10-fold dilutions. Images were taken after 3 days and these experiments were replicated twice with similar results.
(TIF)

S8 Fig. The *ΔFgknr4* strain shows a significant reduction in relative growth rate in response to cell wall stress conditions. A. Wild-type (WT), *ΔFgknr4*, and *ΔFgknr4*::*KNR4* grown on half-strength Potato Dextrose Agar (0.5 PDA) with and without the addition of single stresses. Plates were spotted with 20 μl of 1 x 10^6 conidia/ml conidial suspensions. Images were taken after 3 days. **B.** Colony diameters of WT, *ΔFgknr4*, and *ΔFgknr4*::*KNR4* grown on 0.5 PDA supplemented with calcofluor white (CFW), hydrogen peroxide (H_2O_2), and sodium chloride (NaCl) relative to growth on 0.5 PDA without stress. Significance is denoted as * = $p \leq 0.05$ and ** = $p \leq 0.01$. Significance was determined by a one-way ANOVA followed by Tukey HSD correction.
(TIF)

S9 Fig. Characterisation of conidial length and ascospore production in *ΔFgknr4* and complemented strains. A. Decreased conidial length observed in *ΔFgknr4*. Single conidial images to represent long, middle length, and short conidia across strains. **B**. Distribution of conidial length from N = 50 for WT, *ΔFgknr4*, and *ΔFgknr4*::*KNR4* strains. **C.** Representative perithecia images taken after perithecia induction in carrot agar medium for WT, *ΔFgknr4*, and *ΔFgknr4*::*KNR4* strains. Images taken from above (left panels) and from agar sections placed on slides (right panels) on day 9 and day 17. Scale bar = 500 μm. **D.** Mean perithecia height of WT, *ΔFgknr4*, and *ΔFgknr4*::*KNR4* after 9 and 17 days (N = 40). **E.** Ascospores in intact ascus produced by wild-type (WT), *ΔFgknr4* or *ΔFgknr4*::*KNR4* strains. Scale bar = 10 μM. **F.** Ascospores obtained from squashed perithecia of wild-type (WT), *ΔFgknr4* or *ΔFgknr4*::*KNR4* strains are viable and form germ tubes. Scale bar = 25 μm. Significance is denoted as ** = $p \leq 0.01$. Significance was determined by a one-way ANOVA followed by Tukey HSD correction.
(TIF)

S10 Fig. Additional fluorescent microscopy images of irregular chitin distribution in *ΔFgknr4* conidia. Visualisation of chitin-stained conidia with Wheat Germ Agglutinin Alexa Fluor 488 Conjugate (WGA) in wild-type (WT) **(A)**, *ΔFgknr4* **(B)** and *ΔFgknr4*::*KNR4* **(C).**
(TIF)

S11 Fig. Additional TEM images of abnormal cell wall morphology in *ΔFgknr4* conidia. TEM imaging of wild-type (**A**) and *ΔFgknr4* (**B**) conidia, showing differences in cell wall structure and different magnifications.
(TIF)

S12 Fig. Connections of module F16 candidate genes with cell division and ATP synthesis. Knowledge network demonstrating shared relationships between eight of the 15 candidate genes from module F16. Genes belonging to the candidate gene list are highlighted in yellow.
(TIF)

S13 Fig. High similarity in predicted protein structures of FgKnr4 and ZtKnr4. A. Alphafold3 model of ScKnr4 structure, with residues colours corresponding to pIDDT confidence scores. The predicted template modelling (TM) score is provided next to the structure. **B.** Validation of ScKnr4 Alphafold3 prediction (pink) through alignment with crystal structure of ScKnr4 core (blue). **C.** FgKnr4 Alphafold3 predicted folded structure, with residue colours corresponding to pIDDT confidence scores and displayed with associated pTM score. **D**. ZtKnr4 Alphafold3 predicted folded structure, with residues colours corresponding to pIDDT confidence scores and displayed with associated pTM score. **E.** The alignment of the predicted structures of FgKnr4 (blue) and ZtKnr4 (yellow).
(TIF)

S14 Fig. Significantly decreased necrosis observed on wheat leaves inoculated with *ΔZtknr4*. A. Upper panel includes raw images of detached wheat leaves inoculated with wild-type (WT) *Z. tritici* (IPO323), *ΔZtknr4* mutant strain, and two complemented strains (*ΔZtknr4*::*KNR4-T1* and *T2*) as presented in Fig 9. Images taken at 20 dpi. Lower panel depicts the colour classification of tissue exhibiting healthy (green), chlorosis (yellow), and necrosis (grey) phenotypes as determined by LemnaGrid image analysis system. **B.** Lower panel shows the relative proportion of each leaf surface classified as healthy, chlorosis, or necrosis phenotypes using LemnaGrid image analysis system (N = 3). Significance was determined by a one-way ANOVA followed by a Tukey HSD correction ($p \leq 0.05$).
(TIF)

S15 Fig. *ΔZtknr4* diagnostic PCR and disruption deletion strategy. A. Hygromycin (Hph^R) replacement cassette inserts at *ZtKnr4* locus through homologous recombination via homologous flanks (yellow and white). **B.** Diagnostic PCR demonstrating presence of large insertion fragment in *ΔZtknr4* transformant using Fl1Fwd and Fl2Rev primers.
(TIF)

S1 File. Network module sizes and gene module assignments. Spreadsheet containing sizes of all modules in fungal and wheat networks. 'Fungal module assignments' and 'Wheat module assignments' tabs contain a column with all fungal IDs (RRES v.5 PH-1) or wheat IDs (Column A = IWGSC RefSeq v2.1; Column B = IWGSC RefSeq v1.1) with an adjacent column denoting which module they are clustered in.
(XLSX)

S2 File. *F. graminearum* genes with known phenotypes from the PHI-base database (www.PHI-base.org) in each fungal module. Table provides RRES v5 gene ID, PHI identifier ID

from PHI-base, Uniprot protein ID, gene function, mutant phenotype, experimental technique, author reference, and year published.
(XLSX)

S3 File. *F. graminearum* genes with the highest Module Membership in modules correlated to wheat modules. This supplementary file contains detailed information on the *F. graminearum* genes with the highest module membership within fungal modules that are correlated with wheat modules.
(XLSX)

S4 File. Primer list. Primers used to generate mutant and complemented strains.
(XLSX)

S1 Table. Candidate gene selection in fungal module F16. Table provides details on the 15 candidates within module F16 with the highest module membership (MM) and reason for exclusion from further functional characterisation analysis. This table includes the MM score and associated *p*-values (p.MM), as well as correlation strength to corresponding wheat modules (Cor) and *p*-values (p.Cor).
(XLSX)

Acknowledgments

The authors would like to thank the members of the Rothamsted Horticultural team. The authors also acknowledge use of equipment and advice provided by members of the Rothamsted BioImaging suite.

Author Contributions

Conceptualization: Erika Kroll, Ryan Ames, Martin Urban, Neil A. Brown, Kim Hammond-Kosack.

Data curation: Erika Kroll.

Formal analysis: Erika Kroll.

Investigation: Erika Kroll, Carlos Bayon, Jason Rudd, Victoria J. Armer, Anjana Magaji-Umashankar.

Project administration: Erika Kroll, Jason Rudd, Martin Urban, Neil A. Brown, Kim Hammond-Kosack.

Supervision: Ryan Ames, Martin Urban, Neil A. Brown, Kim Hammond-Kosack.

Validation: Erika Kroll.

Visualization: Erika Kroll.

Writing – original draft: Erika Kroll.

Writing – review & editing: Jason Rudd, Martin Urban, Neil A. Brown, Kim Hammond-Kosack.

References

1. Saldivar SOS. Cereals: Dietary Importance. In: Caballero B, Finglas PM, Toldrá F, editors. Encyclopedia of Food and Health. Oxford: Academic Press; 2016. pp. 703–711. https://doi.org/10.1016/B978-0-12-384947-2.00130–6

2. Shewry PR, Hey SJ. The contribution of wheat to human diet and health. Food Energy Secur. 2015; 4: 178–202. https://doi.org/10.1002/fes3.64 PMID: 27610232
3. Savary S, Willocquet L, Pethybridge SJ, Esker P, McRoberts N, Nelson A. The global burden of pathogens and pests on major food crops. Nat Ecol Evol. 2019; 3: 430–439. https://doi.org/10.1038/s41559-018-0793-y PMID: 30718852
4. O'Donnell K, Kistler HC, Tacke BK, Casper HH. Gene genealogies reveal global phylogeographic structure and reproductive isolation among lineages of *Fusarium graminearum*, the fungus causing wheat scab. Proc Natl Acad Sci. 2000; 97: 7905–7910. https://doi.org/10.1073/pnas.130193297 PMID: 10869425
5. Kanja C, Wood AKM, Baggaley L, Walker C, Hammond-Kosack KE. Cereal-Fusarium interactions: Improved fundamental insights into Fusarium pathogenomics and cereal host resistance reveals new ways to achieve durable disease control. Achieving durable disease resistance in cereals. Chapter 5 In 'Achieving durable disease resistance in cereals' p111-189 Ed R. Oliver, Burleigh Dodds Science Publishing, 2021, ISBN-13: 9781786766014 (chapter ID—ID: 9781801462969)
6. Johns LE, Bebber DP, Gurr SJ, Brown NA. Emerging health threat and cost of Fusarium mycotoxins in European wheat. Nat Food. 2022; 3: 1014–1019. https://doi.org/10.1038/s43016-022-00655-z PMID: 37118304
7. Armer VJ, Kroll E, Darino M, Smith D, Urban M, Hammond-Kosack KE. Navigating the *Fusarium* species complex: Host-Range Plasticity and Genome Variations. Fungal Biol. 2024; 128: 2439–2459. https://doi.org/10.1016/j.funbio.2024.07.004 PMID: 39653491.
8. European Commission. On the presence of deoxynivalenol, zearalenone, ochratoxin A, T-2 and HT-2 and fumonisins in products intended for animal feeding. Off J Eur Union. 2006.
9. EFSA. Risks to human and animal health related to the presence of deoxynivalenol and its acetylated and modified forms in food and feed | EFSA. 11 Sep 2017 [cited 20 May 2024]. Available: https://www.efsa.europa.eu/en/efsajournal/pub/4718
10. AHDB. Risk assessment for fusarium mycotoxins in wheat | AHDB. 2023 [cited 20 May 2024]. Available: https://ahdb.org.uk/mycotoxins
11. Latham RL, Boyle JT, Barbano A, Loveman WG, Brown NA. Diverse mycotoxin threats to safe food and feed cereals. Essays Biochem. 2023; 67: 797–809. https://doi.org/10.1042/EBC20220221 PMID: 37313591
12. Brown NA, Urban M, van de Meene AML, Hammond-Kosack KE. The infection biology of *Fusarium graminearum*: defining the pathways of spikelet to spikelet colonisation in wheat ears. Fungal Biol. 2010; 114: 555–571. https://doi.org/10.1016/j.funbio.2010.04.006 PMID: 20943167
13. Brown NA, Bass C, Baldwin TK, Chen H, Massot F, Carion PWC, et al. Characterisation of the *Fusarium graminearum*-Wheat Floral Interaction. J Pathog. 2011; 2011: e626345. https://doi.org/10.4061/2011/626345 PMID: 22567335
14. Goodwin SB, M'barek SB, Dhillon B, Wittenberg AHJ, Crane CF, Hane JK, et al. Finished genome of the fungal wheat pathogen *Mycosphaerella graminicola* reveals dispensome structure, chromosome plasticity, and stealth pathogenesis. PLoS Genet. 2011; 7: e1002070. https://doi.org/10.1371/journal.pgen.1002070 PMID: 21695235
15. Steinberg G. Cell biology of *Zymoseptoria tritici*: Pathogen cell organization and wheat infection. Fungal Genet Biol. 2015; 79: 17–23. https://doi.org/10.1016/j.fgb.2015.04.002 PMID: 26092785
16. Kema GHJ, Yu D, Frits H. J R, Michael W. S, Robert P. B. Histology of the Pathogenesis of *Mycosphaerella graminicola* in Wheat. Phytopathology. 1996; 86: 777–786.
17. Brown JKM, Chartrain L, Lasserre-Zuber P, Saintenac C. Genetics of resistance to *Zymoseptoria tritici* and applications to wheat breeding. Fungal Genet Biol. 2015; 79: 33–41. https://doi.org/10.1016/j.fgb.2015.04.017 PMID: 26092788
18. Bai G, Su Z, Cai J. Wheat resistance to Fusarium head blight. Can J Plant Pathol. 2018; 40: 336–346.
19. Buerstmayr M, Steiner B, Buerstmayr H. Breeding for Fusarium head blight resistance in wheat—Progress and challenges. Plant Breed. 2020; 139: 429–454. https://doi.org/10.1111/pbr.12797
20. Fones H, Gurr S. The impact of Septoria tritici Blotch disease on wheat: An EU perspective. Fungal Genet Biol. 2015; 79: 3–7. https://doi.org/10.1016/j.fgb.2015.04.004 PMID: 26092782
21. Torriani SFF, Melichar JPE, Mills C, Pain N, Sierotzki H, Courbot M. *Zymoseptoria tritici*: A major threat to wheat production, integrated approaches to control. Fungal Genet Biol. 2015; 79: 8–12. https://doi.org/10.1016/j.fgb.2015.04.010 PMID: 26092783
22. Estep LK, Torriani SFF, Zala M, Anderson NP, Flowers MD, McDonald BA, et al. Emergence and early evolution of fungicide resistance in North American populations of *Zymoseptoria tritici*. Plant Pathol. 2015; 64: 961–971. https://doi.org/10.1111/ppa.12314

23. Lucas JA, Hawkins NJ, Fraaije BA. The evolution of fungicide resistance. Adv Appl Microbiol. 2015; 90: 29–92. https://doi.org/10.1016/bs.aambs.2014.09.001 PMID: 25596029

24. McDonald MC, Renkin M, Spackman M, Orchard B, Croll D, Solomon PS, et al. Rapid Parallel Evolution of Azole Fungicide Resistance in Australian Populations of the Wheat Pathogen *Zymoseptoria tritici*. Appl Environ Microbiol. 2019; 85: e01908–18. https://doi.org/10.1128/AEM.01908-18 PMID: 30530713

25. de Chaves MA, Reginatto P, da Costa BS, de Paschoal RI, Teixeira ML, Fuentefria AM. Fungicide Resistance in *Fusarium graminearum* Species Complex. Curr Microbiol. 2022; 79: 62. https://doi.org/10.1007/s00284-021-02759-4 PMID: 34994875

26. Nelson R. International Plant Pathology: Past and Future Contributions to Global Food Security. Phytopathology. 2020; 110: 245–253. https://doi.org/10.1094/PHYTO-08-19-0300-IA PMID: 31680649

27. Jeger M, Beresford R, Bock C, Brown N, Fox A, Newton A, et al. Global challenges facing plant pathology: multidisciplinary approaches to meet the food security and environmental challenges in the mid-twenty-first century. CABI Agric Biosci. 2021; 2: 20. https://doi.org/10.1186/s43170-021-00042-x

28. Guo L, Ji M, Ye K. Dynamic network inference and association computation discover gene modules regulating virulence, mycotoxin and sexual reproduction in *Fusarium graminearum*. BMC Genomics. 2020; 21: 179.

29. Guo L, Zhao G, Xu J-R, Kistler HC, Gao L, Ma L-J. Compartmentalized gene regulatory network of the pathogenic fungus *Fusarium graminearum*. New Phytol. 2016; 211: 527–541.

30. Langfelder P, Horvath S. WGCNA: an R package for weighted correlation network analysis. BMC Bioinformatics. 2008; 9: 559. https://doi.org/10.1186/1471-2105-9-559 PMID: 19114008

31. Dilks T, Halsey K, De Vos RP, Hammond-Kosack KE, Brown NA. Non-canonical fungal G-protein coupled receptors promote Fusarium head blight on wheat. PLoS Pathog. 2019; 15: e1007666. https://doi.org/10.1371/journal.ppat.1007666 PMID: 30934025

32. Yan X, Tang B, Ryder LS, MacLean D, Were VM, Eseola AB, et al. The transcriptional landscape of plant infection by the rice blast fungus *Magnaporthe oryzae* reveals distinct families of temporally co-regulated and structurally conserved effectors. Plant Cell. 2023; 35: 1360–1385. https://doi.org/10.1093/plcell/koad036 PMID: 36808541

33. Cai H, Yu N, Liu Y, Wei X, Guo C. Meta-analysis of fungal plant pathogen *Fusarium oxysporum* infection-related gene profiles using transcriptome datasets. Front Microbiol. 2022; 13: 970477. https://doi.org/10.3389/fmicb.2022.970477 PMID: 36090060

34. Liu Z, Zhu Z, Huang Y, Nong S, Jiang M, Yi S, et al. Identification of gene modules and hub genes associated with *Colletotrichum siamense* infection in mango using weighted gene co-expression network analysis. BMC Genomics. 2023; 24: 710. https://doi.org/10.1186/s12864-023-09811-6 PMID: 37996781

35. Kugler KG, Siegwart G, Nussbaumer T, Ametz C, Spannagl M, Steiner B, et al. Quantitative trait loci-dependent analysis of a gene co-expression network associated with Fusarium head blight resistance in bread wheat (*Triticum aestivum L.*). BMC Genomics. 2013; 14: 728. https://doi.org/10.1186/1471-2164-14-728 PMID: 24152241

36. Pan Y, Liu Z, Rocheleau H, Fauteux F, Wang Y, McCartney C, et al. Transcriptome dynamics associated with resistance and susceptibility against fusarium head blight in four wheat genotypes. BMC Genomics. 2018; 19: 642. https://doi.org/10.1186/s12864-018-5012-3 PMID: 30157778

37. Zhang L, Zhou X, Li P, Wang Y, Hu Q, Shang Y, et al. Transcriptome Profile of *Fusarium graminearum* Treated by Putrescine. J Fungi. 2022; 9: 60. https://doi.org/10.3390/jof9010060 PMID: 36675881

38. Park J, Lee H-H, Moon H, Lee N, Kim S, Kim J-E, et al. A combined transcriptomic and physiological approach to understanding the adaptive mechanisms to cope with oxidative stress in *Fusarium graminearum*. Microbiol Spectr. 2023; 11: e01485–23. https://doi.org/10.1128/spectrum.01485-23 PMID: 37671872

39. Mateus ID, Masclaux FG, Aletti C, Rojas EC, Savary R, Dupuis C, et al. Dual RNA-seq reveals large-scale non-conserved genotype × genotype-specific genetic reprograming and molecular crosstalk in the mycorrhizal symbiosis. ISME J. 2019; 13: 1226–1238. https://doi.org/10.1038/s41396-018-0342-3 PMID: 30647457

40. Zhang B, Horvath S. A general framework for weighted gene co-expression network analysis. Stat Appl Genet Mol Biol. 2005; 4: Article17. https://doi.org/10.2202/1544-6115.1128 PMID: 16646834

41. Langfelder P, Luo R, Oldham MC, Horvath S. Is My Network Module Preserved and Reproducible? PLOS Comput Biol. 2011; 7: e1001057. https://doi.org/10.1371/journal.pcbi.1001057 PMID: 21283776

42. Breakspear A, Pasquali M, Broz K, Dong Y, Kistler HC. Npc1 is involved in sterol trafficking in the filamentous fungus *Fusarium graminearum*. Fungal Genet Biol. 2011; 48: 725–730. https://doi.org/10.1016/j.fgb.2011.03.001 PMID: 21397712

43. Son H, Seo Y-S, Min K, Park AR, Lee J, Jin J-M, et al. A Phenome-Based Functional Analysis of Transcription Factors in the Cereal Head Blight Fungus, *Fusarium graminearum*. PLoS Pathog. 2011; 7: e1002310. https://doi.org/10.1371/journal.ppat.1002310 PMID: 22028654

44. John E, Singh KB, Oliver RP, Tan K-C. Transcription factor control of virulence in phytopathogenic fungi. Mol Plant Pathol. 2021; 22: 858–881. https://doi.org/10.1111/mpp.13056 PMID: 33973705

45. Zhang Y, Dai Y, Huang Y, Wang K, Lu P, Xu H, et al. The SR-protein FgSrp2 regulates vegetative growth, sexual reproduction and pre-mRNA processing by interacting with FgSrp1 in *Fusarium graminearum*. Curr Genet. 2020; 66: 607–619. https://doi.org/10.1007/s00294-020-01054-2 PMID: 32040734

46. Lu S, Faris JD. *Fusarium graminearum* KP4-like proteins possess root growth-inhibiting activity against wheat and potentially contribute to fungal virulence in seedling rot. Fungal Genet Biol. 2019; 123: 1–13. https://doi.org/10.1016/j.fgb.2018.11.002 PMID: 30465882

47. Vicente I, Quaratiello G, Baroncelli R, Vannacci G, Sarrocco S. Insights on KP4 Killer Toxin-like Proteins of Fusarium Species in Interspecific Interactions. J Fungi. 2022; 8: 968. https://doi.org/10.3390/jof8090968 PMID: 36135693

48. Nguyen T, Kröger C, Bönnighausen J, Schäfer W, Bormann J. The ATF/CREB Transcription Factor Atf1 Is Essential for Full Virulence, Deoxynivalenol Production, and Stress Tolerance in the Cereal Pathogen *Fusarium graminearum*. Mol Plant-Microbe Interact 2013; 26: 1378–1394. https://doi.org/10.1094/MPMI-04-13-0125-R PMID: 23945004

49. Shin Y-K, Kim D-W, Lee S-W, Lee M-J, Gi Baek S, Lee T, et al. Functional roles of all five putative hydrophobin genes in growth, development, and secondary metabolism in *Fusarium graminearum*. Fungal Genet Biol. 2022; 160: 103683. https://doi.org/10.1016/j.fgb.2022.103683 PMID: 35278684

50. Dyer RB, Plattner RD, Kendra DF, Brown DW. *Fusarium graminearum* TRI14 is required for high virulence and DON production on wheat but not for DON synthesis in vitro. J Agric Food Chem. 2005; 53: 9281–9287. https://doi.org/10.1021/jf051441a PMID: 16277434

51. Kimura M, Tokai T, Takahashi-Ando N, Ohsato S, Fujimura M. Molecular and Genetic Studies of *Fusarium* Trichothecene Biosynthesis: Pathways, Genes, and Evolution. Biosci Biotechnol Biochem. 2007; 71: 2105–2123. https://doi.org/10.1271/bbb.70183 PMID: 17827683

52. Cuzick A, Urban M, Hammond-Kosack K. *Fusarium graminearum* gene deletion mutants *map1* and *tri5* reveal similarities and differences in the pathogenicity requirements to cause disease on Arabidopsis and wheat floral tissue. New Phytol. 2008; 177: 990–1000. https://doi.org/10.1111/j.1469-8137.2007.02333.x PMID: 18179606

53. Jansen C, von Wettstein D, Schäfer W, Kogel K-H, Felk A, Maier FJ. Infection patterns in barley and wheat spikes inoculated with wild-type and trichodiene synthase gene disrupted *Fusarium graminearum*. Proc Natl Acad Sci. 2005; 102: 16892–16897. https://doi.org/10.1073/pnas.0508467102 PMID: 16263921

54. Desmond OJ, Manners JM, Stephens AE, Maclean DJ, Schenk PM, Gardiner DM, et al. The Fusarium mycotoxin deoxynivalenol elicits hydrogen peroxide production, programmed cell death and defence responses in wheat. Mol Plant Pathol. 2008; 9: 435–445. https://doi.org/10.1111/j.1364-3703.2008.00475.x PMID: 18705859

55. Arunachalam C, Doohan FM. Trichothecene toxicity in eukaryotes: Cellular and molecular mechanisms in plants and animals. Toxicol Lett. 2013; 217: 149–158. https://doi.org/10.1016/j.toxlet.2012.12.003 PMID: 23274714

56. Brown NA, Evans J, Mead A, Hammond-Kosack KE. A spatial temporal analysis of the *Fusarium graminearum* transcriptome during symptomless and symptomatic wheat infection. Mol Plant Pathol. 2017; 18: 1295–1312. https://doi.org/10.1111/mpp.12564 PMID: 28466509

57. Sertsuvalkul N, DeMell A, Dinesh-Kumar SP. The complex roles of autophagy in plant immunity. FEBS Lett. 2022; 596: 2163–2171. https://doi.org/10.1002/1873-3468.14356 PMID: 35460270

58. Panahi B, Hejazi MA. Weighted gene co-expression network analysis of the salt-responsive transcriptomes reveals novel hub genes in green halophytic microalgae *Dunaliella salina*. Sci Rep. 2021; 11: 1607. https://doi.org/10.1038/s41598-020-80945-3 PMID: 33452393

59. Tominello-Ramirez CS, Muñoz Hoyos L, Oubounyt M, Stam R. Network analyses predict major regulators of resistance to early blight disease complex in tomato. BMC Plant Biol. 2024; 24: 641. https://doi.org/10.1186/s12870-024-05366-0 PMID: 38971719

60. Zheng X, Cairns TC, Ni X, Zhang L, Zhai H, Meyer V, et al. Comprehensively dissecting the hub regulation of PkaC on high-productivity and pellet macromorphology in citric acid producing *Aspergillus*

niger. Microb Biotechnol. 2022; 15: 1867–1882. https://doi.org/10.1111/1751-7915.14020 PMID: 35213792

61. Martin H, Dagkessamanskaia A, Satchanska G, Dallies N, François J. KNR4, a suppressor of *Saccharomyces cerevisiae* cwh mutants, is involved in the transcriptional control of chitin synthase genes. Microbiol Read Engl. 1999; 145 (Pt 1): 249–258. https://doi.org/10.1099/13500872-145-1-249 PMID: 10206705

62. Ghorbel M, Zribi I, Besbes M, Bouali N, Brini F. Catalase Gene Family in Durum Wheat: Genome-Wide Analysis and Expression Profiling in Response to Multiple Abiotic Stress Conditions. Plants. 2023; 12: 2720. https://doi.org/10.3390/plants12142720 PMID: 37514334

63. Zhang Y, Zheng L, Yun L, Ji L, Li G, Ji M, et al. Catalase (CAT) Gene Family in Wheat (*Triticum aestivum L.*): Evolution, Expression Pattern and Function Analysis. Int J Mol Sci. 2022; 23: 542. https://doi.org/10.3390/ijms23010542 PMID: 35008967

64. Andleeb T, Knight E, Borrill P. Wheat NAM genes regulate the majority of early monocarpic senescence transcriptional changes including nitrogen remobilization genes. G3 GenesGenomesGenetics. 2022; 13. https://doi.org/10.1093/g3journal/jkac275 PMID: 36226803

65. Dichtl K, Samantaray S, Wagener J. Cell wall integrity signalling in human pathogenic fungi. Cell Microbiol. 2016; 18: 1228–1238. https://doi.org/10.1111/cmi.12612 PMID: 27155139

66. Hou Z, Xue C, Peng Y, Katan T, Kistler HC, Xu J-R. A mitogen-activated protein kinase gene (MGV1) in *Fusarium graminearum* is required for female fertility, heterokaryon formation, and plant infection. Mol Plant-Microbe Interact. 2002; 15: 1119–1127. https://doi.org/10.1094/MPMI.2002.15.11.1119 PMID: 12423017

67. Yun Y, Liu Z, Zhang J, Shim W-B, Chen Y, Ma Z. The MAPKK FgMkk1 of *Fusarium graminearum* regulates vegetative differentiation, multiple stress response, and virulence via the cell wall integrity and high-osmolarity glycerol signaling pathways. Environ Microbiol. 2014; 16: 2023–2037. https://doi.org/10.1111/1462-2920.12334 PMID: 24237706

68. Martin-Yken H, Dagkessamanskaia A, Basmaji F, Lagorce A, Francois J. The interaction of Slt2 MAP kinase with Knr4 is necessary for signalling through the cell wall integrity pathway in *Saccharomyces cerevisiae*. Mol Microbiol. 2003; 49: 23–35. https://doi.org/10.1046/j.1365-2958.2003.03541.x PMID: 12823808

69. Hoyt MA, Totis L, Roberts BT. *S. cerevisiae* genes required for cell cycle arrest in response to loss of microtubule function. Cell. 1991; 66: 507–517. https://doi.org/10.1016/0092-8674(81)90014-3 PMID: 1651171

70. Hofstad AN, Nussbaumer T, Akhunov E, Shin S, Kugler KG, Kistler HC, et al. Examining the Transcriptional Response in Wheat Near-Isogenic Lines to Infection and Deoxynivalenol Treatment. Plant Genome. 2016; 9: 1–15. https://doi.org/10.3835/plantgenome2015.05.0032 PMID: 27898755

71. Duba A, Goriewa-Duba K, Wachowska U, Głowacka K, Wiwart M. The Associations between Leaf Morphology, Phenylalanine Ammonia Lyase Activity, Reactive Oxygen Species, and Fusarium Resistance in Selected Species of Wheat with Different Ploidy Levels. Plants. 2019; 8: 360. https://doi.org/10.3390/plants8100360 PMID: 31547501

72. Hahlbrock K, Scheel D. Physiology and Molecular Biology of Phenylpropanoid Metabolism. Annu Rev Plant Physiol Plant Mol Biol. 1989; 40: 347–369. https://doi.org/10.1146/annurev.pp.40.060189.002023

73. Kim DS, Hwang BK. An important role of the pepper phenylalanine ammonia-lyase gene (PAL1) in salicylic acid-dependent signalling of the defence response to microbial pathogens. J Exp Bot. 2014; 65: 2295–2306. https://doi.org/10.1093/jxb/eru109 PMID: 24642849

74. Tonnessen BW, Manosalva P, Lang JM, Baraoidan M, Bordeos A, Mauleon R, et al. Rice phenylalanine ammonia-lyase gene OsPAL4 is associated with broad spectrum disease resistance. Plant Mol Biol. 2015; 87: 273–286. https://doi.org/10.1007/s11103-014-0275-9 PMID: 25515696

75. Chen Y, Li F, Tian L, Huang M, Deng R, Li X, et al. The Phenylalanine Ammonia Lyase Gene LjPAL1 Is Involved in Plant Defense Responses to Pathogens and Plays Diverse Roles in *Lotus japonicus*-Rhizobium Symbioses. Mol Plant Microbe Interact. 2017; 30: 739–753. https://doi.org/10.1094/MPMI-04-17-0080-R PMID: 28598263

76. Maher EA, Bate NJ, Ni W, Elkind Y, Dixon RA, Lamb CJ. Increased disease susceptibility of transgenic tobacco plants with suppressed levels of preformed phenylpropanoid products. Proc Natl Acad Sci. 1994; 91: 7802–7806. https://doi.org/10.1073/pnas.91.16.7802 PMID: 8052663

77. Ramaroson M-L, Koutouan C, Helesbeux J-J, Le Clerc V, Hamama L, Geoffriau E, et al. Role of Phenylpropanoids and Flavonoids in Plant Resistance to Pests and Diseases. Molecules. 2022; 27: 8371. https://doi.org/10.3390/molecules27238371 PMID: 36500459

78. Li L, He Z, Pandey GK, Tsuchiya T, Luan S. Functional Cloning and Characterization of a Plant Efflux Carrier for Multidrug and Heavy Metal Detoxification. J Biol Chem. 2002; 277: 5360–5368. https://doi.org/10.1074/jbc.M108777200 PMID: 11739388

79. Perincherry L, Lalak-Kańczugowska J, Stępień Ł. Fusarium-Produced Mycotoxins in Plant-Pathogen Interactions. Toxins. 2019; 11: 664. https://doi.org/10.3390/toxins11110664 PMID: 31739566

80. Li D, Walker E, Francki M. Genes Associated with Foliar Resistance to Septoria Nodorum Blotch of Hexaploid Wheat (*Triticum aestivum L.*). Int J Mol Sci. 2021; 22: 5580. https://doi.org/10.3390/ijms22115580 PMID: 34070394

81. Hill R, Buggs RJA, Vu DT, Gaya E. Lifestyle Transitions in Fusarioid Fungi are Frequent and Lack Clear Genomic Signatures. Mol Biol Evol. 2022; 39. https://doi.org/10.1093/molbev/msac085 PMID: 35484861

82. Zhang Y, Chen W, Shao W, Tan S, Shi D, Ma H, et al. FaSmi1 Is Essential for the Vegetative Development, Asexual Reproduction, DON Production and Virulence of *Fusarium asiaticum*. J Fungi. 2022; 8: 1189. https://doi.org/10.3390/jof8111189 PMID: 36422010

83. Xu M, Wang Q, Wang G, Zhang X, Liu H, Jiang C. Combatting Fusarium head blight: advances in molecular interactions between *Fusarium graminearum* and wheat. Phytopathol Res. 2022; 4: 37. https://doi.org/10.1186/s42483-022-00142-0

84. Jenczmionka NJ, Maier FJ, Lösch AP, Schäfer W. Mating, conidiation and pathogenicity of *Fusarium graminearum*, the main causal agent of the head-blight disease of wheat, are regulated by the MAP kinase gpmk1. Curr Genet. 2003; 43: 87–95. https://doi.org/10.1007/s00294-003-0379-2 PMID: 12695848

85. Urban M, Mott E, Farley T, Hammond-Kosack K. The *Fusarium graminearum* MAP1 gene is essential for pathogenicity and development of perithecia. Mol Plant Pathol. 2003; 4: 347–359. https://doi.org/10.1046/j.1364-3703.2003.00183.x PMID: 20569395

86. Zheng D, Zhang S, Zhou X, Wang C, Xiang P, Zheng Q, et al. The FgHOG1 Pathway Regulates Hyphal Growth, Stress Responses, and Plant Infection in *Fusarium graminearum*. PLOS ONE. 2012; 7: e49495. https://doi.org/10.1371/journal.pone.0049495 PMID: 23166686

87. Cheng W, Song X-S, Li H-P, Cao L-H, Sun K, Qiu X-L, et al. Host-induced gene silencing of an essential chitin synthase gene confers durable resistance to Fusarium head blight and seedling blight in wheat. Plant Biotechnol J. 2015; 13: 1335–1345. https://doi.org/10.1111/pbi.12352 PMID: 25735638

88. Yang P, Yi S-Y, Nian J-N, Yuan Q-S, He W-J, Zhang J-B, et al. Application of Double-Strand RNAs Targeting Chitin Synthase, Glucan Synthase, and Protein Kinase Reduces *Fusarium graminearum* Spreading in Wheat. Front Microbiol. 2021; 12. https://doi.org/10.3389/fmicb.2021.660976 PMID: 34305830

89. Martin-Yken H, François JM, Zerbib D. Knr4: a disordered hub protein at the heart of fungal cell wall signalling. Cell Microbiol. 2016; 18: 1217–1227. https://doi.org/10.1111/cmi.12618 PMID: 27199081

90. Plissonneau C, Hartmann FE, Croll D. Pangenome analyses of the wheat pathogen *Zymoseptoria tritici* reveal the structural basis of a highly plastic eukaryotic genome. BMC Biol. 2018; 16: 5. https://doi.org/10.1186/s12915-017-0457-4 PMID: 29325559

91. Chen H, King R, Smith D, Bayon C, Ashfield T, Torriani S, et al. Combined pangenomics and transcriptomics reveals core and redundant virulence processes in a rapidly evolving fungal plant pathogen. BMC Biol. 2023; 21: 24. https://doi.org/10.1186/s12915-023-01520-6 PMID: 36747219

92. Badet T, Oggenfuss U, Abraham L, McDonald BA, Croll D. A 19-isolate reference-quality global pangenome for the fungal wheat pathogen *Zymoseptoria tritici*. BMC Biol. 2020; 18: 12. https://doi.org/10.1186/s12915-020-0744-3 PMID: 32046716

93. Rudd JJ, Kanyuka K, Hassani-Pak K, Derbyshire M, Andongabo A, Devonshire J, et al. Transcriptome and Metabolite Profiling of the Infection Cycle of *Zymoseptoria tritici* on Wheat Reveals a Biphasic Interaction with Plant Immunity Involving Differential Pathogen Chromosomal Contributions and a Variation on the Hemibiotrophic Lifestyle Definition. Plant Physiol. 2015; 167: 1158–1185. https://doi.org/10.1104/pp.114.255927 PMID: 25596183

94. Dean R, Van Kan JAL, Pretorius ZA, Hammond-Kosack KE, Di Pietro A, Spanu PD, et al. The Top 10 fungal pathogens in molecular plant pathology. Mol Plant Pathol. 2012; 13: 414–430. https://doi.org/10.1111/j.1364-3703.2011.00783.x PMID: 22471698

95. Urban M, Cuzick A, Seager J, Wood V, Rutherford K, Venkatesh SY, et al. PHI-base in 2022: a multi-species phenotype database for Pathogen–Host Interactions. Nucleic Acids Res. 2022; 50: D837–D847. https://doi.org/10.1093/nar/gkab1037 PMID: 34788826

96. Cuzick A, Seager J, Wood V, Urban M, Rutherford K, Hammond-Kosack KE. A framework for community curation of interspecies interactions literature. Graña M, Schuman MC, Etcheverry L, editors. eLife. 2023; 12: e84658. https://doi.org/10.7554/eLife.84658 PMID: 37401199

97. Aamir M, Singh VK, Dubey MK, Meena M, Kashyap SP, Katari SK, et al. *In silico* Prediction, Characterization, Molecular Docking, and Dynamic Studies on Fungal SDRs as Novel Targets for Searching Potential Fungicides Against Fusarium Wilt in Tomato. Front Pharmacol. 2018; 9: 1038. https://doi.org/10.3389/fphar.2018.01038 PMID: 30405403

98. Cools HJ, Hammond-Kosack KE. Exploitation of genomics in fungicide research: current status and future perspectives. Mol Plant Pathol. 2013; 14: 197–210. https://doi.org/10.1111/mpp.12001 PMID: 23157348

99. Machado AK, Brown NA, Urban M, Kanyuka K, Hammond-Kosack KE. RNAi as an emerging approach to control Fusarium head blight disease and mycotoxin contamination in cereals. Pest Manag Sci. 2018; 74: 790–799. https://doi.org/10.1002/ps.4748 PMID: 28967180

100. Mann CWG, Sawyer A, Gardiner DM, Mitter N, Carroll BJ, Eamens AL. RNA-Based Control of Fungal Pathogens in Plants. Int J Mol Sci. 2023; 24: 12391. https://doi.org/10.3390/ijms241512391 PMID: 37569766

101. European Commission. Farm to Fork. 22 Jun 2022 [cited 7 May 2024]. Available: https://ec.europa.eu/commission/presscorner/detail/en/qanda_22_3694

102. Andrews S. FastQC: a quality control tool for high throughput sequence data. 2010. Available: http://www.bioinformatics.babraham.ac.uk/projects/fastqc

103. King R, Urban M, Hammond-Kosack KE. Annotation of *Fusarium graminearum* (PH-1) Version 5.0. Genome Announc. 2017; 5: e01479–16. https://doi.org/10.1128/genomeA.01479-16 PMID: 28082505

104. Zhu T, Wang L, Rimbert H, Rodriguez JC, Deal KR, De Oliveira R, et al. Optical maps refine the bread wheat *Triticum aestivum* cv. Chinese Spring genome assembly. Plant J. 2021; 107: 303–314. https://doi.org/10.1111/tpj.15289 PMID: 33893684

105. Dobin A, Davis CA, Schlesinger F, Drenkow J, Zaleski C, Jha S, et al. STAR: ultrafast universal RNA-seq aligner. Bioinformatics. 2013; 29: 15–21. https://doi.org/10.1093/bioinformatics/bts635 PMID: 23104886

106. Robinson MD, McCarthy DJ, Smyth GK. edgeR: a Bioconductor package for differential expression analysis of digital gene expression data. Bioinforma Oxf Engl. 2010; 26: 139–140. https://doi.org/10.1093/bioinformatics/btp616 PMID: 19910308

107. Lawrence M, Huber W, Pagès H, Aboyoun P, Carlson M, Gentleman R, et al. Software for Computing and Annotating Genomic Ranges. PLOS Comput Biol. 2013; 9: e1003118. https://doi.org/10.1371/journal.pcbi.1003118 PMID: 23950696

108. Love MI, Huber W, Anders S. Moderated estimation of fold change and dispersion for RNA-seq data with DESeq2. Genome Biol. 2014; 15: 550. https://doi.org/10.1186/s13059-014-0550-8 PMID: 25516281

109. Oldham M. M. Transcriptomics: from differential expression to coexpression. The OMICs: applications in neuroscience. Oxford University Press, UK; 2014.

110. Walsh CJ, Batt J, Herridge MS, Mathur S, Bader GD, Hu P, et al. Transcriptomic analysis reveals abnormal muscle repair and remodeling in survivors of critical illness with sustained weakness. Sci Rep. 2016; 6: 29334. https://doi.org/10.1038/srep29334 PMID: 27411715

111. Götz S, García-Gómez JM, Terol J, Williams TD, Nagaraj SH, Nueda MJ, et al. High-throughput functional annotation and data mining with the Blast2GO suite. Nucleic Acids Res. 2008; 36: 3420–3435. https://doi.org/10.1093/nar/gkn176 PMID: 18445632

112. Buchfink B, Xie C, Huson DH. Fast and sensitive protein alignment using DIAMOND. Nat Methods. 2015; 12: 59–60. https://doi.org/10.1038/nmeth.3176 PMID: 25402007

113. Alexa A, Rahnenfuhrer J. Gene set enrichment analysis with topGO. Bioconductor Improv. 2009; 27: 1–26.

114. Cooper L, Elser J, Laporte M-A, Arnaud E, Jaiswal P. Planteome 2024 Update: Reference Ontologies and Knowledgebase for Plant Biology. Nucleic Acids Res. 2024; 52: D1548–D1555. https://doi.org/10.1093/nar/gkad1028 PMID: 38055832

115. Hassani-Pak K, Singh A, Brandizi M, Hearnshaw J, Parsons JD, Amberkar S, et al. KnetMiner: a comprehensive approach for supporting evidence-based gene discovery and complex trait analysis across species. Plant Biotechnol J. 2021; 19: 1670–1678. https://doi.org/10.1111/pbi.13583 PMID: 33750020

116. Sperschneider J, Dodds PN. EffectorP 3.0: Prediction of Apoplastic and Cytoplasmic Effectors in Fungi and Oomycetes. Mol Plant-Microbe Interact. 2022; 35: 146–156. https://doi.org/10.1094/MPMI-08-21-0201-R PMID: 34698534

117. Teufel F, Almagro Armenteros JJ, Johansen AR, Gíslason MH, Pihl SI, Tsirigos KD, et al. SignalP 6.0 predicts all five types of signal peptides using protein language models. Nat Biotechnol. 2022; 40: 1023–1025. https://doi.org/10.1038/s41587-021-01156-3 PMID: 34980915

118. Benjamini Y, Hochberg Y. Controlling the False Discovery Rate: A Practical and Powerful Approach to Multiple Testing. J R Stat Soc Ser B Methodol. 1995; 57: 289–300. https://doi.org/10.1111/j.2517-6161.1995.tb02031.x

119. Sieber CMK, Lee W, Wong P, Münsterkötter M, Mewes H-W, Schmeitzl C, et al. The *Fusarium graminearum* Genome Reveals More Secondary Metabolite Gene Clusters and Hints of Horizontal Gene Transfer. PLOS ONE. 2014; 9: e110311. https://doi.org/10.1371/journal.pone.0110311 PMID: 25333987

120. Gaffoor I, Brown DW, Plattner R, Proctor RH, Qi W, Trail F. Functional analysis of the polyketide synthase genes in the filamentous fungus *Gibberella zeae* (anamorph *Fusarium graminearum*). Eukaryot Cell. 2005; 4: 1926–1933. https://doi.org/10.1128/EC.4.11.1926–1933.2005

121. Wang C, Zhang S, Hou R, Zhao Z, Zheng Q, Xu Q, et al. Functional analysis of the kinome of the wheat scab fungus *Fusarium graminearum*. PLoS Pathog. 2011; 7: e1002460. https://doi.org/10.1371/journal.ppat.1002460 PMID: 22216007

122. Altenhoff AM, Train C-M, Gilbert KJ, Mediratta I, Mendes de Farias T, Moi D, et al. OMA orthology in 2021: website overhaul, conserved isoforms, ancestral gene order and more. Nucleic Acids Res. 2021; 49: D373–D379. https://doi.org/10.1093/nar/gkaa1007 PMID: 33174605

123. Oughtred R, Rust J, Chang C, Breitkreutz B, Stark C, Willems A, et al. The BioGRID database: A comprehensive biomedical resource of curated protein, genetic, and chemical interactions. Protein Sci Publ Protein Soc. 2021; 30: 187–200. https://doi.org/10.1002/pro.3978 PMID: 33070389

124. Cavinder B, Sikhakolli U, Fellows KM, Trail F. Sexual Development and Ascospore Discharge in *Fusarium graminearum*. J Vis Exp JoVE. 2012; 3895. https://doi.org/10.3791/3895 PMID: 22491175

125. Schneider CA, Rasband WS, Eliceiri KW. NIH Image to ImageJ: 25 years of image analysis. Nat Methods. 2012; 9: 671–675. https://doi.org/10.1038/nmeth.2089 PMID: 22930834

126. Yu J-H, Hamari Z, Han K-H, Seo J-A, Reyes-Domínguez Y, Scazzocchio C. Double-joint PCR: a PCR-based molecular tool for gene manipulations in filamentous fungi. Fungal Genet Biol. 2004; 41: 973–981. https://doi.org/10.1016/j.fgb.2004.08.001 PMID: 15465386

127. King R, Urban M, Lauder RP, Hawkins N, Evans M, Plummer A, et al. A conserved fungal glycosyltransferase facilitates pathogenesis of plants by enabling hyphal growth on solid surfaces. PLoS Pathog. 2017; 13: e1006672. https://doi.org/10.1371/journal.ppat.1006672 PMID: 29020037

128. Darino M, Urban M, Kaur N, Machado Wood A, Grimwade-Mann M, Smith D, et al. Identification and functional characterisation of a locus for target site integration in *Fusarium graminearum*. Fungal Biol Biotechnol. 2024; 11: 2. https://doi.org/10.1186/s40694-024-00171-8 PMID: 38409036

129. Huerta-Cepas J, Szklarczyk D, Heller D, Hernández-Plaza A, Forslund SK, Cook H, et al. eggNOG 5.0: a hierarchical, functionally and phylogenetically annotated orthology resource based on 5090 organisms and 2502 viruses. Nucleic Acids Res. 2019; 47: D309–D314. https://doi.org/10.1093/nar/gky1085 PMID: 30418610

130. Letunic I, Bork P. Interactive Tree of Life (iTOL) v6: recent updates to the phylogenetic tree display and annotation tool. Nucleic Acids Res. 2024; gkae268. https://doi.org/10.1093/nar/gkae268 PMID: 38613393

131. Johnson M, Zaretskaya I, Raytselis Y, Merezhuk Y, McGinnis S, Madden TL. NCBI BLAST: a better web interface. Nucleic Acids Res. 2008; 36: W5–W9. https://doi.org/10.1093/nar/gkn201 PMID: 18440982

132. Abramson J, Adler J, Dunger J, Evans R, Green T, Pritzel A, et al. Accurate structure prediction of biomolecular interactions with AlphaFold 3. Nature. 2024; 630: 493–500. https://doi.org/10.1038/s41586-024-07487-w PMID: 38718835

133. Motteram J, Lovegrove A, Pirie E, Marsh J, Devonshire J, van de Meene A, et al. Aberrant protein N-glycosylation impacts upon infection-related growth transitions of the haploid plant-pathogenic fungus *Mycosphaerella graminicola*. Mol Microbiol. 2011; 81: 415–433. https://doi.org/10.1111/j.1365-2958.2011.07701.x PMID: 21623954

134. Keon J, Antoniw J, Carzaniga R, Deller S, Ward JL, Baker JM, et al. Transcriptional adaptation of *Mycosphaerella graminicola* to programmed cell death (PCD) of its susceptible wheat host. Mol Plant-Microbe Interact. 2007; 20: 178–193. https://doi.org/10.1094/MPMI-20-2-0178 PMID: 17313169